



MICS-Asia III: Multi-model comparison and evaluation of aerosol over East Asia

5 Lei Chen^{1,2}, Yi Gao¹, Meigen Zhang^{1,3,4}, Joshua S. Fu⁵, Jia Zhu⁶, Hong Liao^{2,7}, Jialin Li¹, Kan Huang⁵,
Baozhu Ge¹, Xuemei Wang⁸, Yun Fat LAM⁹, Chuan Yao Lin¹⁰, Syuichi Itahashi^{11,12}, Tatsuya
Nagashima¹³, Mizuo Kajino^{14,15}, Kazuyo Yamaji¹⁶, Zifa Wang^{1,3}, Jun-ichi Kurokawa¹⁷

¹State Key Laboratory of Atmospheric Boundary Layer Physics and Atmospheric Chemistry, Institute of Atmospheric Physics, Chinese Academy of Sciences, Beijing, China

10 ²School of Environmental Science and Engineering, Nanjing University of Information Science & Technology, Nanjing 210044, China

³University of Chinese Academy of Sciences, Beijing, China

⁴Center for Excellence in Regional Atmospheric Environment, Institute of Urban Environment, Chinese Academy of Sciences, Xiamen, China

⁵Department of Civil and Environmental Engineering, University of Tennessee, Knoxville, TN 37996, USA

15 ⁶Research Institute of Climatic and Environmental Governance, Nanjing University of Information Science & Technology, Nanjing 210044, China

⁷International Joint Laboratory on Climate and Environmental Change, Nanjing University of Information Science & Technology, Nanjing 210044, China

⁸Institute for Environment and Climate Research, Jinan University, Guangzhou, China

20 ⁹School of Energy and Environment, City University of Hong Kong, Hong Kong

¹⁰Research Center for Environmental Changes, Academia Sinica, Taiwan

¹¹Central Research Institute of Electric Power Industry, Abiko, Chiba 270-1194, Japan;

¹²Department of Marine, Earth, and Atmospheric Sciences, North Carolina State University, Raleigh, NC 27607, USA

¹³National Institute for Environmental Studies, Tsukuba, Japan

25 ¹⁴Meteorological Research Institute, Japan Meteorological Agency, Tsukuba, 305-0052, Japan

¹⁵Faculty of Life and Environmental Sciences, University of Tsukuba, Tsukuba, 305-8577, Japan

¹⁶School of Science and Engineering, Meisei University, Hino, Tokyo 191-8506, Japan

¹⁷Asia Center for Air Pollution Research, 1182 Sowa, Nishi-ku, Niigata, Niigata, 950-2144, Japan

30 *Correspondence to:* M.G. Zhang (mgzhang@mail.iap.ac.cn)

Abstract. Fourteen chemical transport models (CTMs) participate in the MICS–Asia Phase III Topic 1. Their simulation results are compared with each other and with an extensive set of measurements, aiming to evaluate the current multi–scale air quality models’ ability in simulating aerosol species and to document similarities and differences among model performances, also to reveal the characteristics of aerosol chemical components over big cities in East Asia. In general, all
35 participant models can reproduce the spatial distribution and seasonal variability of aerosol concentrations in the year 2010, and multi–model ensemble mean (EM) shows better performance than most individual models, with Rs ranging from 0.65 (NO₃⁻) to 0.83 (PM_{2.5}). Underestimations of BC (NMB=-17.0%), SO₄²⁻ (NMB=-19.1%) and PM₁₀ (NMB=-32.6%) are simulated by EM, but positive biases are shown in NO₃⁻ (NMB=4.9%), NH₄⁺ (NMB=14.0%) and PM_{2.5} (NMB=4.4%). Simulation results of BC, OC, SO₄²⁻, NO₃⁻ and NH₄⁺ among CTMs are in good agreements, especially over polluted areas,



5

such as the eastern China and the northern part of India. But large coefficients of variations ($CV > 1.5$) are also calculated over arid and semi-arid regions. This poor consistency among CTMs may attribute to their different processing capacities for dust aerosols. According to the simulation results in the six Asian cities from EM, different air-pollution control plans should be made due to their different major air pollutants in different seasons. Although a more considerable capacity for reproducing the concentrations of aerosol chemical compositions and their variation tendencies is shown in current CTMs by comparing statistics (e.g. RMSE and R) between MICS-Asia Phase II and Phase III, detailed process analysis and a fully understanding of the source-receptor relationship in each process may be helpful to explain and to reduce large diversities of simulated aerosol concentrations among CTMs, and these may be the potential development directions for future modeling studies in East Asia.

10



1 Introduction

Rapid urbanization and industrialization have stimulated economic growth and population expansion during the last several decades in East Asia (Spence et al., 2008; Yan et al., 2016; Chen et al., 2016), but also brought about the noticeable degradation of ecological environment at the same time (Hall 2002; Han et al., 2014; Yue et al., 2017). Significant increase in atmospheric aerosol loading, especially from anthropogenic emissions, can exert much influence on weather (Cowan et al., 2013; Gao et al., 2015a), climate (Wang et al., 2016a), air quality (Gao et al., 2016a), and even human health (Carmichael et al., 2009). For example, aerosols can enhance the absorption and scattering of solar radiation to modify the thermodynamic structure of the atmospheric boundary layer (Ding et al., 2016; Petaja et al., 2016), can act as cloud condensation nuclei and ice nuclei to alter cloud properties and precipitation (Lohmann and Diehl, 2006; Wang, 2013a), can trigger visibility deterioration and result in haze events (Singh and Dey, 2012; Li et al., 2014). In addition, fine particulate matter with aerodynamic diameters smaller than 2.5 μm ($\text{PM}_{2.5}$) can also enter into the alveoli to cause severe cardiovascular diseases, respiratory diseases and even lung cancer (Pope and Dockery, 2006; Gao et al., 2015a). All these impacts have attracted considerable attention among the public and policy makers in East Asia, and the research on aerosols has become a hot topic which is frequently reported and deeply studied during recent years.

In order to better understand the properties of atmospheric aerosols and their impacts, chemical transport models (CTMs) can be a critical tool, and they have been drawn up and applied to study various air pollution issues all over the world. For example, a fully coupled online Weather Research and Forecasting/Chemistry (WRF/Chem) model was developed by Grell et al. (2005) and was used to study the aerosol–radiation–cloud feedbacks on meteorology and air quality (Gao et al., 2014; Zhang et al., 2015a; Qiu et al., 2017); a Models–3 Community Multi–scale Air Quality (CMAQ) modeling system was designed by the US Environmental Protection Agency (Byun and Ching, 1999) and was carried out to address acid deposition, visibility and haze pollution issues (Zhang et al., 2006; Han et al., 2014; Fan et al., 2015); a nested air quality prediction model system (NAQPMS) was developed by the Institute of Atmospheric Physics, Chinese Academy of Science (IAP/CAS) (Wang et al., 2001) for targeting at reproducing the transport and evolution of atmospheric pollutants in Asia (Li et al., 2012a; Wang et al., 2013c; Li et al., 2017a); a global three–dimensional chemical transport model (GEOS–CHEM) was first presented by Bey et al. (2001) and was applied to study the source sector contribution, long–range transport and the prediction of future change in ozone and aerosol concentrations (Liao et al., 2006; Li et al., 2016b; Zhu et al., 2017).

Although significant advances have taken place in these CTMs, how to accurately reproduce and/or predict the concentrations and the distributions of atmospheric pollutants is still a challenge, with the problems of inaccurate emission inventories, poorly represented initial and boundary conditions, and imperfect physical, dynamical and chemical parameterizations (Carmichael et al., 2008). Meanwhile, most CTMs are designed to focus on the air quality over developed countries, such as Europe and America, rather than in Asia, and the assumptions or look–up tables used in models may not be suitable to simulate the Asian environment (Gao et al., 2018). Therefore, before providing scientifically meaningful



information and answering “what-if” questions for policy makers, model performances must be first evaluated. Hayami et al. (2008) and Mann et al. (2014) pointed out that multi-model ensemble mean (EM) tends to show better performance than most participant models when comparing with observations, and large variation in simulation results can be found among participant models, which may be caused by using different parameters and calculation methods in each CTM (Carmichael et al., 2002; Hayami et al., 2008; Wang et al., 2008; Holloway et al., 2008). In order to develop a better common understanding of the performance and uncertainties of CTMs in East Asia applications, and to acquire a more mature comprehension of the properties of atmospheric aerosols and their impacts in East Asia, a model inter-comparison study should be initiated, and Model Inter-Comparison Study for Asia (MICS-Asia) gives an opportunity to investigate these questions. Meanwhile, model inter-comparison study in East Asia is very limited (Phadnis et al., 1998; Kiley et al., 2003; Han et al., 2008) and far more efforts are needed.

The MICS-Asia project was initiated in 1998. In the first phase of MICS-Asia (MICS-Asia Phase I), the primary target is to study the long-range transport and deposition of SO_4^{2-} in East Asia by analyzing the submitted simulation results from eight CTMs. Source-receptor relationship, contributions of wet/dry pathways for remove, and the influence of model structure and parameters on simulation capability are also estimated. More details can be found in Carmichael et al. (2002). As an extension of Phase I, MICS-Asia Phase II includes more chemical species of concern, such as sulfur, nitrogen and ozone. This broader collaborative study examined four different periods, encompassing two different years and three different seasons (March, July, and December in 2001, and March in 2002). Simulation results are from nine different regional modeling groups. Detailed information about this project can be found on the overview paper of Carmichael et al. (2008). In 2010, the MICS-Asia III project was launched. As a part of EANET additional research activity and a continuing research of MICS-Asia series, three topics are discussed, including comparison and evaluation of current multi-scale air quality models (Topic 1), development of reliable emission inventories for CTMs in Asia (Topic 2), and interactions between air quality and climate changes (Topic 3).

This manuscript focuses on the first topic of the MICS-Asia Phase III, and tries to present and summary the following three objectives, which mainly specialize in the analysis topic of aerosol species. Firstly, a comprehensive evaluation of the strengths and weaknesses of current multi-scale air quality models for simulating particulate matter (PM) is provided against extensive measurements from in-situ and satellites, aiming to show the capability of participant models. Secondly, the diversity of simulated aerosol concentrations among participant models is analyzed including suggestions about how to reduce uncertainties in simulation results, which can be used as a reference for future development and improvement of models. Thirdly, characteristics of aerosol chemical components over analyzed regions in East Asia are revealed, which may be helpful to provide confidence for future investigation of aerosol impacts on regional climate in East Asia.

The descriptions of model configurations, model inputs, analyzing area and observation data are presented in Section 2. The evaluation for model performance and the inter-comparison between participant models are shown in Section 3. The conclusions and discussions are presented in Sections 4.



2 Inter-comparison framework

2.1 Model description

Fourteen modeling groups participated in MICS-Asia phase III Topic 1. Basic information about the configurations of each model is summarized in Table 1. Among these models, five different kinds of chemistry modules are applied, including
5 CMAQ (Community Multiscale Air Quality), WRF-Chem (Weather Research and Forecasting Model coupled with Chemistry), NAQPMS (nested air quality prediction model system), NHM-Chem (non-hydrostatic mesoscale model coupled with chemistry transport model), and GEOS-Chem (global three-dimensional chemical transport model). For CMAQ, there are four different versions: CMAQ5.0.2 (M1 and M2), CMAQ5.0.1 (M3), CMAQ4.7.1 (M4, M5 and M6), and CMAQ4.6 (M14). For WRF-Chem, there are also four different versions: WRF-Chem3.7.1 (M7), WRF-Chem3.6.1 (M8),
10 WRF-Chem3.6 (M9), and WRF-Chem3.5.1 (M10). Only one version is used for NAQPMS (M11), NHM-Chem (M12) and GEOS-Chem (version 9.1.3, M13).

The settings of gas phase chemistry and aerosol chemistry are key components of chemical transport models, and can influence the simulation results significantly (Cuchiara et al., 2014). The gas chemistry of SAPRC 99 (the 1999 Statewide Air Pollution Research Center) was used in M1, M2, M4, M5, M6, M12 and M14. It is a detailed mechanism for the
15 gas-phase atmospheric reactions of volatile organic compounds (VOCs) and oxides of nitrogen (NO_x) in urban and regional atmospheres. It includes 76 species reacting in 214 reactions (Carter, 2000). CB05 (2005 Carbon Bond) chemical mechanism was used in M3. It is a condensed mechanism of atmospheric oxidant chemistry that provides a basis for computer modeling studies of ozone, particulate matter (PM), visibility, acid deposition and air toxics issues, with 51 species and 156 reactions (Yarwood et al., 2005). M9 and M10 used RADM2 (Regional Acid Deposition Model, version 2) gas chemistry mechanism.
20 The inorganic species included in the RADM2 are 14 stable species, 4 reactive intermediates, and 3 abundant stable species. Atmospheric organic chemistry is represented by 26 stable species and 16 peroxy radicals (Stockwell et al., 1990). It has been extensively used in atmospheric models to predict concentrations of oxidants and other air pollutants. Based on RADM2, Regional Atmospheric Chemistry Mechanism (RACM) created by Stockwell et al. (1997) is capable of modeling a wide variety of complex and practical situations, from the Earth's surface to the troposphere and from remote to polluted
25 urban conditions. This mechanism was used in M7 and M8, including 17 stable inorganic species, 4 inorganic intermediates, 32 stable organic species, and 24 organic intermediates, with up to 237 reactions. M11 used CBMZ (Carbon-Bond Mechanism version Z) and this mechanism extends the original framework of CBM-IV to function properly at larger spatial and longer timescales, with 67 species and 164 reactions (Zaveri and Peters, 1999). In order to have a comprehensive understanding of factors controlling tropospheric ozone, one major theme of the gas chemistry mechanism used in M13
30 (GEOS-Chem) is the simulation of ozone- NO_x -hydrocarbon chemistry, which includes about 80 species and 300 chemical reactions (Bey et al., 2001; Zhu et al., 2017).

The Aero5/Aero6 aerosol module with ISORROPIA aerosol thermodynamics v1.7/v2 were used in M1, M2, M3, M4, M5, M6, M11, M12 and M14. It is designed to simulate the thermodynamic equilibrium of inorganic species (e.g. NH_4^+ ,



sodium, chloride, NO_3^- , SO_4^{2-} and water), and all the aerosol particles are assumed to be internally mixed (Nenes et al, 1998). Meanwhile, these modules use a weighted average approach to approximate the aerosol composition in mutual deliquescence regions, which can speed up the solution time. The Aero5 ISORROPIA (v1.7) was mainly used in CMAQ model version before 5.0, after which the second version (ISORROPIA (v2)) was implemented. The main change in ISORROPIA v2 is to introduce thermodynamics of crustal species such as Ca^{2+} , K^+ and Mg^{2+} (Fountoukis and Nenes, 2007), and the corresponding impacts are mainly on the gas–particle partitioning of NO_3^- and NH_4^+ in areas with high dust emissions. Wang et al. (2012b) pointed out that the updated treatment of crustal species in ISORROPIA v2 can reduce fine mode of particle matter over polluted areas. The aerosol module used in M7 and M9 is MADE (Modal Aerosol Dynamics Model for Europe) (Ackermann et al., 1998) for the inorganic fraction, and the Secondary Organic Aerosol Model (SORGAM) (Schell et al., 2001) for the carbonaceous secondary fraction. For MADE/SORGAM, the modal approach with three log–normally distributed modes (nuclei, accumulation and coarse mode) is implemented in the WRF–Chem model. Similar as the aerosol chemistry of MADE/SORGAM, secondary organic aerosols (SOA) was also simulated by the advanced Volatility Basis Set (VBS) approach in M8 (Tuccella et al., 2015). The bulk GOCART (Goddard Global Ozone Chemistry Aerosol Radiation and Transport) aerosol module (originally developed by NASA) used in M10 can output fourteen aerosol species, including hydrophobic and hydrophilic organic carbon (OC1 and OC2) and black carbon (BC1 and BC2), SO_4^{2-} , dust in five particle–size bins, and sea salt in four particle–size bins. This mechanism can provide an integrated sectional scheme for dust emission and aerosol advection, but indirect effects and wet scavenging/deposition schemes regarding cloud interactions are not supported (Chin et al., 2000). Aerosol species considered in GEOS–Chem (M13) include SO_4^{2-} (Park et al., 2004), NO_3^- (Pye et al., 2009), NH_4^+ , OC and BC (Park et al., 2003), mineral dust (Fairlie et al., 2007), and sea salt (Alexander et al., 2005).

As is known to all that meteorological fields has a profound impact on air quality, and aerosol compositions can affect weather and climate directly by changing clouds, radiation, and precipitation (Forkel et al., 2015). In order to simulate the concentrations of air pollutants, meteorological models and chemistry transport models can be implemented either offline or online (Kong et al., 2015). Offline modeling implies that CTM is run after the meteorological simulation is completed, and the chemistry feedbacks on meteorology are not considered. Online modeling allows coupling and integration of some of the physical and chemical components (Baklanov et al., 2014). According to the extent of online coupling, there are two ways of coupling: online integrated coupling (meteorology and chemistry are simulated in one model using the same grid and using one main time step for integration) and online access coupling (meteorology and chemistry are independent, but information can be exchanged between meteorology and chemistry on a regular basis) (Baklanov et al., 2014). Among these participating models, M4, M5, M6, M12, M13 and M14 are offline models. M1, M2, M3, and M11 are online access models. M7, M8, M9 and M10 are online integrated models. Different coupling methods can cause different simulation results due to the interactions among aerosol, weather and climate. Even though using the same coupling way, different parameterizations can also cause uncertainties. More details about the model configurations are summarized in Table 1 and other MICS–Asia Phase III companion papers.



5

For aerosol species, modeling variables of BC, OC, SO_4^{2-} , NO_3^- , NH_4^+ , $\text{PM}_{2.5}$, PM_{10} and AOD from the fourteen participant models, as listed in Table 2, are requested to upload to a public server. But no data are acquired from M10, and all simulation results from M3 are incredible. Therefore, only twelve models are analyzed in this manuscript. Meanwhile, M5, M6 and M8 did not submit simulated AOD. M13 did not submit simulated PM_{10} . M7 did not submit OC. Neither BC nor OC was submitted from M9.

2.2 Information about model inputs

Based on the experience of Phase I and Phase II, all participant models in Phase III Topic 1 are required to use common meteorological fields, emission inventories and boundary conditions in order to reduce the potential diversity that may be caused by input dataset.

10

The meteorological fields are outputted from the Weather Research and Forecasting Model (WRF v3.4.1) using the National Center for Environmental Prediction (NCEP) Final Analysis (FNL) data with $1^\circ \times 1^\circ$ spatial resolution and 6 h temporal interval, but M10, M12, M13 and M14 choose to use others. In M10, the initial and lateral boundary meteorological fields are run by WRF (v3.5.1) driven by Modern Era Retrospective-analysis for Research and Applications (MERRA) reanalysis dataset. The outputs from the Japan Meteorological Agency (JMA) non-hydrostatic mesoscale model (NHM) are initialized in M12 (Kajino et al., 2012). M13 is driven by assimilated meteorological data from the Goddard Earth Observing System (GEOS) of NASA's Global Modeling and Assimilation Office (Chen et al., 2009; Li et al., 2016c). Although initial and lateral boundary conditions are taken from the same NCEP FNL data, three dimensional meteorological fields used in M14 are simulated by Regional Atmospheric Modeling System (RAMS) (Zhang et al., 2002, 2007; Han et al., 2009, 2013). These different atmospheric forcing dataset may result in differences in simulated circulation fields and other meteorological variables, which can further influence the concentrations and the distributions of simulated air pollutants.

15

20

25

30

All models utilized a common emission inventory, which includes anthropogenic, biogenic, biomass burning, air and ship, and volcano emissions. The anthropogenic emission dataset over Asia, named MIX, is developed by harmonizing five regional and national emission inventories with a mosaic approach. These five inventories are REAS2 (REAS inventory version 2.1 for the whole of Asia, Kurokawa et al., 2013), MEIC (the Multi-resolution Emission Inventory for China developed by Tsinghua University), PKU-NH₃ (a high-resolution NH₃ emission inventory by Peking University, Huang et al., 2012), ANL-India (an Indian emission inventory developed by Argonne National Laboratory, Lu et al., 2011), and CAPSS (the official Korean emission inventory form the Clean Air Policy Support System, Lee et al., 2011). The MIX inventory includes ten species (SO_2 , NO_x , CO, CO_2 , NMVOC (non-methane volatile organic compounds), NH_3 (ammonia), BC (black carbon), OC (organic carbon), $\text{PM}_{2.5}$ and PM_{10}) in each sector (power, industry, residential, transportation, and agriculture), and is developed for the year 2010 with monthly temporal resolution and 0.25 degree spatial resolution. More details can be found in Li et al. (2017b). Weekly and diurnal profiles of the anthropogenic emissions provided by the MICS-Asia organizers are used in model simulations, including the emission factors for the first seven vertical levels (Fig. S1). Hourly biogenic emissions quantified by the Model of Emissions of Gases and Aerosols from Nature (MEGAN) version



2.04 (Guenther et al., 2006) are provided for the whole MICS–Asia phase III simulation period. To drive MEGAN, meteorological variables (e.g. solar radiation, air temperature, soil moisture) and land cover information (e.g. leaf area index (LAI), plant functional types (PFTs)) are necessary inputs, and these data are obtained from WRF simulations and MODIS (Moderate Resolution Imaging Spectroradiometer) products, respectively. Biomass burning emissions are processed by re-gridding the Global Fire Emissions Database (GFED) version 3 (van der Werf et al., 2010). Hourly fraction of biomass burning emission for each day during the entire year is also provided. The aircraft and shipping emissions are based on the 2010 HTAPv2 (Hemispheric Transport of Air Pollution) emission inventory (0.1 by 0.1 degree) (Janssens–Maenhout et al., 2015). Daily volcanic SO₂ emissions can be collected from the AEROCOM program (<http://www-lscedods.cea.fr/aerocom/AEROCOM/HC/volc/>, Diehl et al., 2012; Stuefer et al., 2013). The spatial distribution of the merged emissions of SO₂, NO_x and PM_{2.5} from anthropogenic, biogenic, biomass burning, air and ship, and volcano emissions are shown in Fig. 1. Similar spatial patterns can be found among these species, with high values in eastern China and northern India.

Chemical concentrations at the top and lateral boundary conditions from 3–hourly global CTM outputs of CHASER (run by Nagoya University, Sudo et al., 2002a; Sudo et al., 2002b) and GEOS–Chem (run by University of Tennessee, <http://acmg.seas.harvard.edu/geos/>) are provided by MICS–Asia III. CHASER model is run with 2.8°×2.8° horizontal resolution and 32 vertical layers, and GEOS–Chem is run with 2.5°×2° horizontal resolution and 47 vertical layers.

A reference model computational domain recommended by MICS–Asia organizers covers the region of (15.4°S–58.3°N, 48.5°E–160.2°E) using 180×170 grid points at 45 km horizontal resolution, but most participant models employ different extents of the region as shown in Fig. 2. In order to minimize the influence from lateral boundary conditions and to cover most high–profile areas of East Asia, a common domain is designed in this manuscript as shown in Fig. 2 with the red solid line. For M13 and M14, missing value is used to fill the grids beyond their simulation domains. In this common domain, five different regions are assigned with different colors (Fig. 3): Region_1, filled with blue, contains Korean Peninsula and Japan; Region_2, filled with cyan, contains China only; Region_3, filled with chartreuse, contains Mongolia and parts of Russia; Region_4, filled with orange, contains most countries in Southeast Asia; Region_5, filled with purple, contains most countries in South Asia. Therefore, modeling results in different geographical sub–regions of East Asia can be analyzed and compared with each other to show the simulation performance of current CTMs.

The whole year 2010 is chosen as the study period for MICS–Asia Phase III Topic 1. During 2010, many important weather events have been documented, such as extreme summer heat waves and widespread monsoon precipitation which affected many Asian countries (Chen et al., 2015; Jongman et al., 2015); a super dust storm originated from Gobi Desert in March 2010 and swept across vast areas of East Asia (Li et al., 2011); a winter severe haze episode occurred in the North China Plain (NCP) in January 2010 (Gao et al., 2016b). All these provide good opportunities to analyze the characteristics of the spatial and temporal distribution of aerosol concentrations over East Asia.



2.3 Observation data

In order to make an international common understanding and improve air pollution modeling in East Asia, observation data (e.g. SO_4^{2-} , NO_3^- , NH_4^+ , $\text{PM}_{2.5}$ and PM_{10}) at 39 sites of the Acid Deposition Monitoring Network in East Asia (EANET) are used to evaluate the model performance, as did in MICS–Asia Phase II. Common quality assurance and quality control standards promoted by the ADORC (Acid Deposition and Oxidant Research Center) are adopted among these EANET stations to guarantee high quality dataset. More information about the EANET dataset can be found at <http://www.eanet.asia/index.html>. In addition to the EANET data, monthly measurements of air pollutants (e.g. SO_2 , NO_2 , $\text{PM}_{2.5}$ and PM_{10}) over the Beijing–Tianjin–Hebei (BTH) region (19 sites) and the Pearl River Delta (PRD) region (13 sites) provided by the China National Environmental Monitoring Center (CNEMC) are also used to compare with the simulation results from participating models.

As is known to all, China has been experiencing air pollutions with high concentrations of fine particles, and recent studies highlight the importance of secondary aerosols in the formation of haze episodes (Liu et al., 2013; Sun et al., 2016; Chen et al., 2018). However, observed aerosol components (e.g. SO_4^{2-} , NO_3^- and NH_4^+) in inland China are only available at one EANET site (the Hongwen site). In order to make the evaluation of the model performance more credible, observed monthly/seasonal/yearly BC, SO_4^{2-} , NO_3^- , NH_4^+ and $\text{PM}_{2.5}$ concentrations at several Chinese stations (five stations for BC, thirteen stations for SO_4^{2-} , NO_3^- and NH_4^+ , and twenty-two stations for $\text{PM}_{2.5}$) are collected from published documents (Chen et al., 2012; Li, 2012b; Liu, 2012; Meng et al., 2012; Shao, 2012; Wang et al., 2012a; Xu, 2012; Xie et al., 2013; Yu, 2013; Zhao et al., 2013; Tao et al., 2014; Wang, 2014a; Li, 2015; Sun et al., 2015; Wang et al., 2015; Zhang, 2015b; Lai et al., 2016; Li et al., 2016a; Wang et al., 2016b; Deng et al., 2016; Yao et al., 2016).

The Aerosol Robotic Network (AERONET), a ground–based remote–sensing aerosol network consisting of worldwide automatic sun– and sky–scanning spectral radiometers (Holben et al., 1998), provides the aerosol optical depth (AOD) products at 440 nm and 675 nm, which are used to calculate the AOD at 550 nm with the Angström exponent. The AERONET Level 2.0 monthly AOD data (cloud–screened and quality–assured data) at thirty–three sites are utilized in this study. Meanwhile, satellite–retrieved 550 nm AOD products from the Moderate Resolution Imaging Spectroradiometer (MODIS) and Multi–angle Imaging Spectroradiometer (MISR) are also used to compare with the simulations.

Figure 3 shows the locations of all the observational sites (marked with black dots) for each measured species. Most SO_4^{2-} , NO_3^- and NH_4^+ monitoring sites are located in China, Japan and the Southeast Asia, only two in Mongolia and four in Russia. Except three PM_{10} sites are located in the Southeast Asia, other PM observational stations are in China and Japan. Detailed information about all these ground–level stations can be found in Table S1 and Table S2.

In general, the wide variety of measurements from in–situ and satellites used in this manuscript can allow for a rigorous and comprehensive evaluation of model performances.



3 Results and discussions

3.1 Model evaluation

Following the objective of MICS–Asia Phase III Topic 1, comparisons of aerosol concentrations (BC, SO_4^{2-} , NO_3^- , NH_4^+ , $\text{PM}_{2.5}$ and PM_{10}), including aerosol optical depth (AOD), between observations and simulations (results from individual models and EM) are presented to evaluate the performance of current multi–scale air quality models in East Asia simulation, as well as to analyze the differences between participant models.

3.1.1 Evaluation for aerosol particles

Figure 4 illustrates the observed and simulated ground level annual mean concentrations of BC, SO_4^{2-} , NO_3^- , NH_4^+ , $\text{PM}_{2.5}$ and PM_{10} . EMs, derived from averaging all the available participating models (except M3 and M10) are also presented to exhibit a composite of model performances. Monitoring sites are categorized into five regions (Region_1, Region_2, Region_3, Region_4 and Region_5) by their geographic locations as listed in Table S1, and are separated by vertical dashed lines in Fig. 4. Normalized mean biases (NMBs) between observations and EMs in each defined region and the whole analyzed domain are calculated.

Analyzing Fig. 4(a), we can find that most models show good skills in simulating the BC concentration and its spatial distribution, with high values over North China Plain (NCP) and Yangtze River Delta (YRD) regions, and low values over Central West of China. But the NMB for EM is -15.8% . This underestimation may be attributed to the large negative bias from all participant models at site 24 (the Gucheng site). This station is located in the Hebei province, which is an industrial city, where air pollution is serious and BC emission is large (Wang et al., 2016c). Due to the low reactivity of BC in the atmosphere, the high uncertainty of BC in current emission inputs (Hong et al., 2017; Li et al., 2017b) may explain this underestimation.

For SO_4^{2-} , observations are relative low in Region_1 (mean value is $3.8 \mu\text{g m}^{-3}$), Region_3 (mean value is $2.5 \mu\text{g m}^{-3}$) and Region_4 (mean value is $3.5 \mu\text{g m}^{-3}$), and most models perform well over these regions. But nearly all observed annual mean SO_4^{2-} concentrations in Region_2 are larger than $10 \mu\text{g m}^{-3}$ (mean value is $16.9 \mu\text{g m}^{-3}$), and most models fail to reproduce the high magnitude. A large variance can be found among models, e.g. M14 obviously overpredict ground–level SO_4^{2-} , especially in Region_1, whereas M7 and M9 consistently underpredict SO_4^{2-} at nearly all sites. Huang et al. (2014) and Zheng et al. (2015) pointed out that heterogeneous chemistry on the surface of aerosol can enhance the production of SO_4^{2-} , especially under polluted conditions (Li et al., 2018). But the mechanism of the heterogeneous uptake of SO_2 on deliquesced aerosols may have not been updated in M7 and M9. The model EM better agrees with measurements of SO_4^{2-} concentration than most participating models, and EM can well reproduce the spatial distribution of SO_4^{2-} . However, underestimation is found in each defined region, especially in Region_2 (NMB= -43.5%) and Region_3 (NMB= -35.3%).

Similar spatial distribution of observed NO_3^- concentrations can also be found in Fig. 4(c). The mean values of observed NO_3^- concentrations in each region are $1.5 \mu\text{g m}^{-3}$ (Region_1), $13.4 \mu\text{g m}^{-3}$ (Region_2), $0.6 \mu\text{g m}^{-3}$ (Region_3) and



1.8 $\mu\text{g m}^{-3}$ (Region_4), respectively. Analyzing the performance of each model, a significant overestimation (underestimation) is simulated by M9 (M7 and M8), especially in Region_2. This may result from the biases of model calculation of heterogeneous reactions (Kim et al., 2014), gas-aerosol phase partitioning (Brunner et al., 2014), and deposition (Shimadera et al., 2014). For example, N_2O_5 hydrolysis is considered in M9, but not in M7 and M8. Su et al. (2016) pointed out that the hydrolysis of N_2O_5 can lead up to 21.0% enhancement of NO_3^- , especially over polluted regions. This may partly explain the differences of simulated NO_3^- concentrations between M7, M8 and M9. Another major possible reason to explain this extreme underestimation of NO_3^- in M7 and M8 is their incorrect treatments of the NH_3 emission inputs. As the main alkaline gas in the atmosphere, NH_3 can react with H_2SO_4 and HNO_3 , which are produced by the oxidation of SO_2 and NO_x , to form $(\text{NH}_4)_2\text{SO}_4$ and NH_4NO_3 , and makes a significant contribution to the formation of secondary inorganic aerosols (Pan et al., 2016; Zhang et al., 2018). The low simulated concentrations of NH_4^+ , as shown in Fig. 4(c) and Fig. 17, can also support this explanation. Although the NMB calculated in Region_All (Region_All means the whole analyzed region) for EM is only -1.1%, EM systematically overpredicts observations in Region_1 (NMB=45.2%) and Region_3 (NMB=38.2%), but underpredicts in Region_2 (NMB=-0.7%) and Region_4 (NMB=-44.9%).

Simulated NH_4^+ concentrations are associated with the amounts of SO_4^{2-} and NO_3^- , but model predictions can reproduce the measurements relatively well with NMBs ranging from -7.8% to 32.0%. In general, the calculated NMB in Region_All is 4.0%. However, obviously overestimation (underestimation) is also simulated by M14 (M7 and M8), especially in Region_2.

On average, the observed $\text{PM}_{2.5}$ concentration in Region_2 is larger than $50 \mu\text{g m}^{-3}$, while the mean value is only about $10 \mu\text{g m}^{-3}$ in Region_1. All participating models can generally capture this spatial distribution pattern. However, significant underestimation is found at the three remote stations (site 1, 2 and 7) in Region_1 with the NMB of -39.0% for EM. Similar negative bias can also be found in Ikeda et al. (2013), who compared CMAQ (v4.7.1) simulation results against observations from the same remote monitoring stations (Rishiri and Oki) throughout the same year 2010. And Ikeda et al. (2013) pointed that the underestimation of organic aerosols caused the negative bias of simulated $\text{PM}_{2.5}$ mass concentration. In Region_2, the NMB for EM is -10.0%.

For PM_{10} , the mean observed concentrations in each region are $26.6 \mu\text{g m}^{-3}$ (Region_1), $114.4 \mu\text{g m}^{-3}$ (Region_2) and $38.1 \mu\text{g m}^{-3}$ (Region_4), respectively. Comparing with observations, an underprediction tendency can be found among almost all participating models except M14, which predicts higher concentrations in Region_1, especially at coastal sites, such as site 1(Rishiri), 2(Ochiishi), 4(Sadoseki), 7(Oki) and 14(Cheju). The high-value anomalies along coastal areas simulated by M14 can also be found in Fig. 19, and the positive bias may be caused by the emission and gravitational settling of sea salt. As Monahan and Muircheartaigh (1980) pointed out that sea salt emissions can be enhanced in the surf zone due to increased number of wave breaking events, and the degree of the enhancement highly depends on the 10 m wind speed used in the whitecap coverage parameterization. Meanwhile, higher wind speed at coastal stations was simulated by M14 (RAMSCMAQ) when comparing with observations from previous related studies (Han et al., 2013; Han et al., 2018). In addition, a gravitational settling mechanism of coarse aerosols from upper to lower layers is added in M14, and the net



effect of this update is an increase in PM_{10} concentrations, especially near coastal areas impacted by sea spray (Nolte et al., 2015). In general, the NMB for EM in Region_All is -31.0% .

Figure 5 and Figure 6 show the seasonality of observed and simulated aerosol particle mass concentrations, including BC, SO_4^{2-} , NO_3^- , NH_4^+ , $PM_{2.5}$ and PM_{10} . All simulations and observations are grouped into five defined regions as illustrated in Fig. 3, with the modeling results sampled at the corresponding observation sites before averaging together. Individual models are represented by the thin grey lines, with the grey shaded areas indicating their spread. The thick black line is the EM. The red solid line is the observational mean and the dashed red lines represent one standard deviation for each group of stations. The correlation coefficients (Rs) for EMs versus the monthly observations are calculated in each panel, and the normalized mean biases (NMBs) in each season (spring: from March to May; summer: from June to August; autumn: from September to November; winter: January, February and December) for EM are also given.

The measured BC concentrations in Region_2 exhibit an obvious seasonal variation with the minimum ($\sim 3.5 \mu g m^{-3}$) during spring and summer, and the maximum ($\sim 8 \mu g m^{-3}$) during late autumn and winter. All participating models can capture this observed seasonality quite well, and all modeling results are within the standard deviation of the observations, but a large inter-model variation is found, especially in winter when BC concentration is high. Different coupling ways between meteorological and chemical modules, as listed in Table 1, can be used to explain this variation. As Gao et al. (2015b), Briant et al. (2017) and Huang et al. (2018) concluded that the online integrated models can simulate higher BC concentrations than offline models, especially during polluted periods. The correlation coefficient for EM is 0.73.

In each month, the mean-observed $PM_{2.5}$ concentration over Region_2 is larger than that in Region_1. This is because the emissions of primary aerosol and precursors in China are larger than that in Japan and Korean Peninsula (Fig. 1). Nearly all models tend to underpredict the magnitude of $PM_{2.5}$ in Region_1 during the whole simulation period with the range of NMB from -44.3% (in winter) to -22.7% (in summer) for EM. The seasonality of modeling $PM_{2.5}$ concentration in Region_2 is better with the R of 0.69 for EM, comparing with the correlation coefficient ($R=0.40$) in Region_1. In general, the R for EM in Region_All is 0.83 and the NMB ranges from -2.2% to 13.9% among four seasons.

The characteristics of the observed PM_{10} concentrations in Region_1, Region_2 and Region_4 are similar, with the maximum in March and November, and the minimum during summer. M14 consistently overestimates the PM_{10} concentrations in Region_1 for all periods, while others fall within the standard deviation of the observations. The simulated PM_{10} concentrations in Region_2 show less diversity, but nearly all models peak 2 months later. A distinctive seasonality can be found in Region_4 with the maximum (nearly $80 \mu g m^{-3}$) in March, but most models cannot reproduce the maximum. This is because the GFED substantially underestimated the biomass burning emissions over Southeast Asia (Fu et al., 2012), especially during March–April when most intense biomass burning occurred in Myanmar, Thailand and other Southeast Asian countries (Huang et al., 2012), and the emission bias is mainly due to the lack of agricultural fires (Nam et al., 2010). Finally, a weak PM_{10} seasonality was simulated by EM with R of 0.58 in Region_4. In Region_all, although consistently underestimation is found during the whole simulation period with NMB ranging from -40.8% to -25.2% for EM, the seasonal cycle can be well captured by EM with R of 0.78.



For SO_4^{2-} , NO_3^- and NH_4^+ in Region_1, the seasonal variation characteristics of observations are not obvious, with the annual mean values of $\sim 4 \mu\text{g m}^{-3}$ for SO_4^{2-} , $1.5 \mu\text{g m}^{-3}$ for NO_3^- and $1 \mu\text{g m}^{-3}$ for NH_4^+ , respectively. A large inter-model spread of simulated SO_4^{2-} is shown in Fig. 6(a1) with the maximum in June. Double-peak curve is displayed in Fig. 6(b1) with the maximums in May and November, and most models significantly overpredict the NO_3^- concentration, especially in summer. Unlike SO_4^{2-} and NO_3^- , the simulated monthly NH_4^+ concentrations from most models are within the standard deviation of observations, and the R for multi-model mean is highest with the value of 0.74. In Region_2, the observed monthly mean aerosol components are only available at one EANET site (the Hongwen site, located in the eastern coastal area of China), and the seasonality of observed SO_4^{2-} , NO_3^- and NH_4^+ from this station is obvious with the maximum in spring and winter, and the minimum in later summer and early autumn. Nearly all models tend to underpredict these concentrations, but the EM captures the seasonal cycles relative well with Rs of 0.57 for SO_4^{2-} , 0.85 for NO_3^- and 0.86 for NH_4^+ , respectively. In Region_3, the observed maximum concentrations of SO_4^{2-} and NH_4^+ are in winter, but most models cannot reproduce the increasing tendency in the late autumn and the early winter, and then fail to capture the seasonality (Rs of 0.20 for SO_4^{2-} , 0.34 for NO_3^- and 0.18 for NH_4^+ , respectively). This may due to the low emissions of primary aerosol and precursors in Region_3, as shown in Fig.1. In Region_4, the simulated concentrations of SO_4^{2-} , NO_3^- and NH_4^+ are fairly good when compared with the measurements. The Rs of EM are 0.73 for SO_4^{2-} , 0.63 for NO_3^- and 0.73 for NH_4^+ . Meanwhile, the model diversities are small. Generally, in Region_All, EM can reproduce the magnitudes of observed SO_4^{2-} , NO_3^- and NH_4^+ fairly well during the whole simulation period, as well as the seasonal variation characteristics.

As mentioned above that observed monthly mean concentrations of aerosol compositions in China are only available at one EANET station (site 17, the Hongwen station) with missing values in June and October. In order to make the evaluation of simulated aerosol chemical components over China more comprehensive, observed seasonal mean concentrations of SO_4^{2-} , NO_3^- and NH_4^+ collected from published documents are also used to compare with simulations as shown in Fig. 7. M2 and M14 show the reasonable SO_4^{2-} concentrations in the four seasons, while others fail to reproduce the high observed SO_4^{2-} concentrations, with the NMBs ranging from -79.4% (M7) to -28.0% (M12). Most models overestimate the concentrations of NO_3^- and NH_4^+ in China, but significant underestimation can be found in M7 and M8 (NMBs are larger than -70%). The underestimation may be due to their incorrect treatments of the NH_3 emission inputs, including missing aqueous-phase and heterogeneous chemistry reactions or the implementations of a different gas phase oxidation mechanism (RACM gas phase chemistry mechanism). In fact, the underestimation of SO_4^{2-} and the overestimation of NO_3^- may be the common phenomenon in most current air quality models (Wang et al., 2013b; Gao et al., 2014; Huang et al., 2014; Zheng et al., 2015), and some hypotheses should be deeply tested in future to reduce the deviation, such as (1) missing oxidation mechanism of SO_2 may lead to low concentration of SO_4^{2-} , which allows for excess NO_3^- in the presence of ammonia, (2) there is an issue with NO_x partitioning or missing NO_x sink. Analyzing the results from ensemble mean, EM shows better performance than participating models, with NMBs of -46.0% for SO_4^{2-} , 1.9% for NO_3^- and 13.1% for NH_4^+ .

Seinfeld and Pandis (2016) pointed out that chemical productions of SO_4^{2-} and NO_3^- are mainly from the gas-phase or



liquid-phase oxidation of SO₂ and NO₂. Therefore, further comparisons of observed and simulated seasonal cycle of SO₂ and NO₂ in Region_2 and annual mean concentrations of SO₂ and NO₂ at corresponding stations are shown in Fig. S2 and Fig. S3, respectively. From Fig. S2, participating models can generally reproduce the seasonality of the two gases, with Rs of 0.61 for SO₂ and 0.65 for NO₂, respectively. But overestimations (underestimations) of SO₂ (NO₂) are found in most simulation periods, not only in China, but also in other defined regions (Fig. S3), and the overestimation (underestimation) of SO₂ (NO₂) can be used to explain the underestimation (overestimation) of simulated SO₄²⁻ (NO₃⁻).

3.1.2 Evaluation for aerosol optical depth

The seasonal cycle of simulated aerosol optical depth (AOD) at 550 nm is also compared with measurements at thirty-three AERONET stations. Only nine participating models (M1, M2, M4, M7, M9, M11, M12, M13 and M14) submitted their simulated AOD values, and the EM is calculated by these nine models. From Fig. 8 we can find that most models tend to overpredict AOD during the whole simulation period in Region_1, Region_2 and Region_3 with NMBs of 74.0%, 38.8% and 107.0% for EM, respectively. In Region_4, an obvious seasonality is observed with the maximum in spring and the minimum in summer. Models can capture the seasonality well, although underestimation is found in spring. The R for EM is 0.65 and the NMB is -8.7% in Region_4. Model bias in Region_5 is smaller with the NMB of -4.2% for EM, but a quite weak seasonality is simulated with underestimation in spring and summer, and overestimation in autumn and winter. Generally, simulated AOD values lie within a standard deviation of the observations in Region_All with a slight overestimation in autumn and winter. The EM can reproduce the seasonal cycle with R of 0.68, and the NMB for EM is 18.7%.

Figure 9 presents the spatial distribution of 550 nm AOD retrieved by MODIS and simulated by the nine models. In this study, MODIS AOD is collected by the Terra and Aqua satellites during the whole year of 2010. AOD observed from AERONET stations are also shown. In order to quantify the ability of each model to reproduce the spatial distribution of aerosol particles, spatial correlation coefficients are given in the bottom left corner of each panel. Analyzing the observations from MODIS, we can conclude that AOD values are higher in central and eastern China including Sichuan province with the maximum over 1.0. High values can also be found in the north India. Due to dust events happened in spring, AOD values over the Taklimakan area are also large (~0.5). Comparing with MODIS AOD, almost all models can reproduce the spatial distribution feature with high values in China and India and low values in other countries. The Rs range from 0.78 to 0.86. The model EM captures the AOD spatial variability better with R of 0.87.

Figure 10 shows the differences between model results and MODIS AOD to further discuss the performance of participant models. We can conclude that most models tend to underestimate the AOD values in the eastern coastal regions of China and the north regions of India where the emissions are large, in addition to the Taklimakan area in China where dust particles can be lifted up frequently. Meanwhile, overestimation is simulated by M2 and M14, especially in the Sichuan province of China. Generally, mean biases averaged over the whole analyzed region for the nine models ranges from -0.16 to 0.05, and the mean bias for EM is -0.08.



Figure 11 shows the annual mean 550 nm AOD from each available model averaged over the five defined regions (Region_1 to Region_5) and the whole analyzed domain (Region_All), together with the measured AOD retrieved from MODIS and MISR. AOD averaged over the corresponding AEROENT stations in each region are also shown. Analyzing the observations, MODIS AOD is the highest and AERONET value is the lowest. This difference can be explained by the systematic biases in MODIS retrievals due to the impacts of aerosol model assumptions and cloud contamination (Hauser et al., 2005; Toth et al., 2013), in addition to the difference in number of days used to calculate the average (Li et al., 2009). Meanwhile, observations from AERONET sites only represent special samples in each region. Similar results can also be found in other researches (Alpert et al., 2012; Li et al., 2014; Liu et al., 2014). Analyzing the simulations, multi-model mean can generally reproduce the magnitude of observations within a factor from 0.5 to 1.6, especially comparing with AOD values retrieved from MISR, and the EMs in the five defined regions are 0.29 ± 0.12 for Region_1, 0.34 ± 0.26 for Region_2, 0.21 ± 0.09 for Region_3, 0.18 ± 0.17 for Region_4 and 0.23 ± 0.13 for Region_5, respectively. But the inter-model spread is large by a factor of 2–5 in magnitude, and in most regions, AOD values simulated by M4 are lowest, M2 and M11 show the highest.

3.1.3 Statistics for aerosol particles and aerosol optical depth

Table 3 shows the statistics of correlation coefficient (R), normalized mean bias (NMB) and root-mean squared error (RMSE) for BC, SO_4^{2-} , NO_3^- , NH_4^+ , $\text{PM}_{2.5}$, PM_{10} and AOD. Results from twelve models and EM are compared with available observations. Best results are set to be bold with underline.

It can be found that all models are able to generally capture the variability of BC in China, with Rs ranging from 0.65 of M5 to 0.80 of M8, but nearly all models tend to underestimate the BC concentration, except M1 and M2. The maximum negative deviation is simulated by M5 with NMB of -54.9% , while the maximum positive deviation is from M2 with NMB of 12.7% . All the RMSEs are less than the mean BC observation ($5.0 \mu\text{g m}^{-3}$). Comparing to the observed SO_4^{2-} , most models fail to reproduce the magnitude of concentrations. NMBs range from -67.7% of M7 to 69.3% of M14, and the NMB for EM is -19.1% , meaning underprediction is found in most participating models. This may be caused by the imperfect mechanism of gas-phase and liquid-phase oxidation of SO_2 , in addition to the missing heterogeneous reactions on the surface of aerosol particles in most current multi-scale air quality models (Huang et al., 2014, Zheng et al., 2015; Fu et al., 2016). But most models can capture the variation of SO_4^{2-} with Rs ranging from 0.46 of M14 to 0.76 of M13. For NO_3^- , Rs vary from 0.29 of M8 to as high as 0.65 of EM. M5 exhibits the largest correlation (0.65) and the smallest NMB (-1.7%) along all models. Although a high R (0.64) is calculated by M9, the NMB is the largest (125.7%). All RMSEs are larger than the measured NO_3^- ($1.7 \mu\text{g m}^{-3}$), meaning a relative poor performance for current air quality models to simulate the NO_3^- concentration in East Asia. For NH_4^+ , underestimation can be found in M4, M7 and M8, while the others tend to overestimate the NH_4^+ concentration. Although all RMSEs are larger than the observed NH_4^+ concentration of $1.1 \mu\text{g m}^{-3}$, most models can capture the variability, with Rs ranging from 0.34 of M8 to 0.75 of M9. Generally, the multi-model mean matches the observed values with R of 0.71, NMB of 14.0% and RMSE of $1.11 \mu\text{g m}^{-3}$, respectively. Although significant



underpredictions are found in PM_{10} (NMBs range from -55.7% of M5 to -16.9% of M9, except M14), and the inter-model spread of $PM_{2.5}$ is large (NMBs range from -26.5% of M13 to 46.0% of M14), simulated $PM_{2.5}$ and PM_{10} variations are well correlated with measurements ($R_s > 0.60$), and the RMSEs are all smaller than the averaged measurements ($51.4 \mu\text{g m}^{-3}$ for $PM_{2.5}$ and $80.7 \mu\text{g m}^{-3}$ for PM_{10} , respectively). For AOD, large positive deviation can be found in M2, M9, M11, M13 and M14, although their R_s are all larger than 0.5. M4 and M7 show the large negative deviation with NMBs of -28.5% and -21.8% , respectively. But their RMSEs are relative small (0.16 for M4 and 0.18 for M7). Generally, the R, NMB and RMSE for EM are 0.68, 18.7% and 0.14, respectively.

3.2 Inter-comparison between MICS-Asia Phase II and Phase III

The main purpose of MICS-Asia Phase III Topic 1 is to assess the ability of current multi-scale air quality models to reproduce air pollutant concentrations. In order to reflect how well the performance of air quality models in East Asia simulation after undergoing substantial development during last several years, statistics (e.g. RMSE and R) for observed and simulated SO_4^{2-} , NO_3^- and NH_4^+ from MICS-Asia Phase II and Phase III are compared in Fig. 12.

The statistics of MICS-Asia Phase II are taken from Hayami et al. (2008), in which observed monthly mean aerosol composition concentrations were monitored with high completeness at fourteen EANET stations in March, July and December 2001 and March 2002, while model-predicted monthly surface concentrations are from eight regional CTMs. Notably, NO_3^- and NH_4^+ used in Hayami et al. (2008) are total NO_3^- (= gaseous HNO_3 + particulate NO_3^-) and total NH_4^+ (= gaseous NH_3 + particulate NH_4^+), respectively. More detailed information can be found in Hayami et al. (2008).

Analyzing the RMSEs in Fig. 12, we can conclude that the medians (interquartile ranges) for SO_4^{2-} , NO_3^- and NH_4^+ are $3.60 \mu\text{g m}^{-3}$ ($3.24, 4.01 \mu\text{g m}^{-3}$ 25th/75th percentiles), $2.76 \mu\text{g m}^{-3}$ ($2.49, 2.96 \mu\text{g m}^{-3}$ 25th/75th percentiles) and $1.28 \mu\text{g m}^{-3}$ ($1.21, 1.47 \mu\text{g m}^{-3}$ 25th/75th percentiles) in Phase III, respectively. Although the medians (except NH_4^+) are a little bit larger than that in Phase II, the ranges are quite smaller, meaning similar aerosol concentrations can be simulated by current multi-scale models. Meanwhile, the medians of the correlations of SO_4^{2-} , NO_3^- , and NH_4^+ in Phase III, including the upper and lower quartiles, are all significantly larger than that in Phase II, meaning the better performance of current air quality models in reproducing the variation tendency of observations.

Although the participating models (8 verses 12 CTMs), evaluation sites (14 verses 31 EANET stations) and simulation periods (4 months verses 1 year) are different between Phase II and Phase III, the compared results of statistics calculated from observations and simulations can still generally show that better performance is found in current multi-scale air quality models than those participating in MICS-Asia Phase II when reproducing the concentrations of aerosol particles and their variety characteristics.

3.3 Inter-comparison between participant models

Figure 13 to Figure 19 show the spatial distribution of simulated BC, OC, SO_4^{2-} , NO_3^- , NH_4^+ , $PM_{2.5}$ and PM_{10}



concentrations from each participating model and the multi-model EM. The coefficient of variation (hereinafter, CV), defined as the standard deviation of the models divided by their mean, is also calculated. The larger CV, the lower the consistency is among participating models.

For BC, high values ($> 5 \mu\text{g m}^{-3}$) can be successfully simulated by all models (except M5) over the eastern China including the Sichuan province, and the northeast part of India. Meanwhile, areas with high concentrations ($> 5 \mu\text{g m}^{-3}$) are nearly consistent with the regions where CV values are relative low (< 0.5). However, large CV (> 1.0) is shown over the Himalayas and the Indian Ocean. This is probably due to the different vertical resolutions in addition to the different transmission mechanisms. Generally, the CVs in the five defined regions are all smaller than 0.6. All participant models show similar spatial distribution and magnitude of OC, except M5 and M8 with obvious low values over China and India. Analyzing the results from EM, the highest concentrations are simulated over the Eastern China, Sichuan Province and the northern part of India with values larger than $10 \mu\text{g m}^{-3}$. CVs are lower than 0.7 in these relative high-concentration areas, while high CV values (> 1.5) are shown over the Tibetan Plateau and low-latitude oceans. For SO_4^{2-} , NO_3^- and NH_4^+ , high concentrations are centered in the eastern China and the north India, including the Sichuan province of China. However, apparent low SO_4^{2-} (NO_3^- and NH_4^+) concentrations are simulated by M7 and M9 (M7 and M8). Meanwhile, noticeable high concentrations of SO_4^{2-} are simulated by M14, especially along coastal regions. CVs of SO_4^{2-} and NH_4^+ averaged over the five defined regions are all lower than 0.7, and maximum CVs are all smaller than 1.5, indicating simulation results are in good agreement. But a poor consistency is shown among simulated NO_3^- concentrations with CVs larger than 0.6 over each defined region. For $\text{PM}_{2.5}$ and PM_{10} , high values are simulated by M9, M12 and M14 over arid and semi-arid regions, such as the Taklimakan Desert and the Gobi Desert, where dust events were observed in spring. The CVs in these regions are quite large (over 1.5), which means different processing capacities for dust aerosols and different dust emission mechanisms used among these models. M14 also shows higher values of PM_{10} over coastal regions than other models. This may be caused by the inadequate simulation results of sea salt.

3.4 Characteristics of chemical compositions of particulate matter

Figure 20 shows the chemical compositions of simulated particulate matter (PM) averaged over the whole analyzed area in 2010 from each participating model and the multi-model EM. PM_{10} includes $\text{PM}_{2.5}$ and OTHER2, while $\text{PM}_{2.5}$ is composed of BC, OC, SO_4^{2-} , NO_3^- , NH_4^+ and OTHER1. Notably, OTHER2 cannot be calculated in M13 because PM_{10} has not been submitted. OC is not available in M7, so we leave it into OTHER1. BC and OC are not available in M9 and these concentrations are grouped into OTHER1.

From Fig. 20 we can find that the simulated concentrations of PM_{10} vary a lot by about a factor of 4 among models, with the highest in M9 ($46.5 \mu\text{g m}^{-3}$) and the lowest in M5 ($11.5 \mu\text{g m}^{-3}$). This large spread can be explained by the differences in simulated concentrations of OTHER2, which is mainly composed of dust aerosol and sea salt aerosol. Generally, the mean PM_{10} concentration from EM is $24.1 \mu\text{g m}^{-3}$, including $0.9 \mu\text{g m}^{-3}$ (3.5%) for BC, $2.5 \mu\text{g m}^{-3}$ (10.3%) for OC, $3.1 \mu\text{g m}^{-3}$ (12.9%) for SO_4^{2-} , $2.7 \mu\text{g m}^{-3}$ (11.3%) for NO_3^- , $1.7 \mu\text{g m}^{-3}$ (7.1%) for NH_4^+ , $6.4 \mu\text{g m}^{-3}$ (26.7%) for



OTHER1 and $6.8 \mu\text{g m}^{-3}$ (28.2%) for OTHER2. For $\text{PM}_{2.5}$, the regional mean concentration from EM is $17.3 \mu\text{g m}^{-3}$, with an inter-model range from $9.7 \mu\text{g m}^{-3}$ of M5 to $28.1 \mu\text{g m}^{-3}$ of M14. Except OTHER1, the major compositions in $\text{PM}_{2.5}$ in East Asia are SO_4^{2-} (18.0%), NO_3^- (15.7%) and OC (14.4%).

Aerosol chemical compositions in six high-profile cities in East Asia (Beijing, Shanghai, Guangzhou, Delhi, Seoul and Tokyo) simulated by each participating model and the multi-model EM are shown in Fig. 21. High values of $\text{PM}_{2.5}$ and PM_{10} in Beijing, Shanghai, Guangzhou and Delhi can be simulated by nearly all models, while relative small concentrations are presented in Seoul and Tokyo. For each city, a large spread of PM concentrations can be found among models, this is mainly caused by the differences of the simulated concentrations of OTHER1 and OTHER2. In other words, although common emissions are used, different physical-chemical parameterizations can cause large uncertainties in transmission and remove processes of aerosols, including the emission processes of dust and sea salt. Analyzing the ratios of aerosol compositions to PM (PM_{10} and $\text{PM}_{2.5}$) from simulation results of EM in Fig. 22, the sums of the contributions of BC, OC, SO_4^{2-} , NO_3^- and NH_4^+ in Beijing, Shanghai, Guangzhou and Delhi are all less than those in Seoul and Tokyo. Among these components in $\text{PM}_{2.5}$ (Fig. 22(b1–b6)), except OTHER1, NO_3^- is the major component in Beijing (20.7%) and Delhi (23.6%), while SO_4^{2-} is the major one in Guangzhou (22.2%). Similar contributions of SO_4^{2-} and NO_3^- can be found in Shanghai, Seoul and Tokyo. All these suggest that different air-pollution control plans should be made in different metropolitans. For seasonal variations of $\text{PM}_{2.5}$ concentrations (Fig. 22(c1–c6)), the highest values in Beijing ($107.6 \mu\text{g m}^{-3}$), Shanghai ($87.5 \mu\text{g m}^{-3}$), Guangzhou ($59.9 \mu\text{g m}^{-3}$) and Delhi ($108.7 \mu\text{g m}^{-3}$) are all simulated in winter. This can be explained by their high emissions in winter. However, in Tokyo, the highest $\text{PM}_{2.5}$ concentration appears in summer ($21.8 \mu\text{g m}^{-3}$) and the lowest is in winter ($10.3 \mu\text{g m}^{-3}$). In Seoul, $\text{PM}_{2.5}$ concentrations are comparable during the four seasons.

4 Conclusion and Discussion

As part of the research of the first topic in MICS-Asia Phase III, this manuscript mainly focuses on the analysis topic of aerosol species, and tries to present and summary the following three objectives: (1) provide a comprehensive evaluation of the strengths and weaknesses of current multi-scale air quality models against extensive measurements from in-situ and satellites, (2) analyze the diversity of simulated aerosol concentrations among participant models, and (3) reveal the characteristics of key aerosol chemical components over high-profile cities in East Asia. Fourteen regional modeling groups participating in Topic 1 are required to simulate aerosol species using common meteorological fields, emission inventories and boundary conditions during the entire year of 2010 in East Asia. Model predictions are compared with each other, and with measurements of BC, OC, SO_4^{2-} , NO_3^- , NH_4^+ , $\text{PM}_{2.5}$ and PM_{10} . Aerosol optical depth is also rigorously evaluated against observations from AERONET, MODIS and MISR. Note that all simulation results from M3 are incredible, and no data is gained from M10. Meanwhile, M5, M6 and M8 did not submit simulated AOD. M13 did not submit simulated PM_{10} . M7 did not submit OC. Neither BC nor OC was submitted from M9.

Comparisons against monthly observations from EANET and CNEMC demonstrate that all participant models can



reproduce the spatial–temporal evolution of the concentrations of aerosol species, and multi–model EM shows better performance than most models, with Rs ranging from 0.65 (NO_3^-) to 0.83 ($\text{PM}_{2.5}$) for EM. Differences between simulations and observations can also be found during the analyzing period, such as SO_4^{2-} is underestimated by participant models (except M12 and M14) with NMBs ranging from -67.7% to -1.6% , while most models overestimate the concentrations of NO_3^- and NH_4^+ , and the NMBs are 4.9% and 14.0% for EM, respectively. These biases may be caused by the imperfect mechanisms of gas–phase or liquid–phase oxidation of SO_2 and NO_2 , including the missing heterogeneous chemistry reactions in most current multi–scale air quality models. Notably, significant underestimations of NO_3^- and NH_4^+ in M7 and M8 may be due to their incorrect treatments of the NH_3 emission inputs. The inter–model spread of simulated $\text{PM}_{2.5}$ is large, with NMBs ranging from -26.5% of M13 to 46.0% of M14, and nearly all models underestimate the $\text{PM}_{2.5}$ concentrations in Region_1. Inaccurate aerosol long–range transport from high–concentration source regions (e.g. Region_2) to low–concentration downstream areas (e.g. Region_1) may explain this bias. Underestimations of PM_{10} are also simulated over the whole analyzed regions, and the NMB of EM in Region_All is -32.6% for PM_{10} . For AOD, participating models can reasonably reproduce the spatial variability and the seasonal cycle when comparing with observations from AERONET and MODIS. But underestimations are found along the eastern coastal regions of China and the northern regions of India, where anthropogenic emissions are large, in addition to the Taklimakan area where dust particles can be frequently lifted up. Different capacities to process dust particles and different dust schemes used in participating models may cause the bias.

In order to reveal how well the CTMs can reproduce the characteristics of aerosol species in East Asia after undergoing substantial development during recent years, statistics for observed and simulated SO_4^{2-} , NO_3^- and NH_4^+ from MICS–Asia Phase II and Phase III are compared. Results obviously show that the variation ranges of RMSEs for each species among participating models in Phase III become smaller, meaning similar concentrations are simulated. Meanwhile the median of the correlations, including the upper and lower quartiles, is larger, indicating the evolution characteristics of observations are better simulated. All these demonstrate a more considerable capacity for reproducing aerosol concentrations and their variation tendencies in current air quality models.

The coefficient of variation is frequently used to quantify the inter–model deviation, and a large CV is calculated over the arid and semi–arid regions, where dust events were observed in the spring of 2010. The poor consistency may be associated with the different dust emission mechanisms used in participating models. But in general, simulation results of BC, OC, SO_4^{2-} , NO_3^- and NH_4^+ are all in good agreement, especially over the relative highly polluted areas, such as the eastern and northeast China, and the northeast part of India.

According to the simulation results from EM, the highest $\text{PM}_{2.5}$ concentrations of Beijing ($107.6 \mu\text{g m}^{-3}$), Shanghai ($87.5 \mu\text{g m}^{-3}$), Guangzhou ($59.9 \mu\text{g m}^{-3}$) and Delhi ($108.7 \mu\text{g m}^{-3}$) are shown in winter, mainly due to the high emissions and unfavorable weather conditions in winter. But the highest in Tokyo appears in summer ($21.8 \mu\text{g m}^{-3}$). $\text{PM}_{2.5}$ concentrations are comparable during the four seasons in Seoul. Analyzing the ratios of chemical compositions to $\text{PM}_{2.5}$ in these cities, NO_3^- is the major component in Beijing (20.7%) and Delhi (23.6%), SO_4^{2-} is the major one in Guangzhou (22.2%), similar contributions of SO_4^{2-} and NO_3^- are calculated in Shanghai, Seoul and Tokyo. All these suggest that different



air–pollution control plans should be made according to the main contaminants in different cities.

MICS–Asia project gives an opportunity to understand the performance of air quality models in East Asia applications. Analyzing the results concluded above, in order to reduce the diversities of simulated aerosol concentrations among participant models, more efforts are needed for future modeling studies. For example, process analysis scheme should be developed and implemented in air quality models, and individual process, such as advection, diffusion, emission, dry deposition, wet scavenging, gas–phase chemistry and cloud chemistry should be isolated to make a quantitative attribution for the cause of the differences between model predictions. Fully understanding of the source–receptor relationship in each process for a given aerosol species can be helpful to revise parameterization schemes for better simulation capability. Meanwhile, more observations should be collected and used in the next MICS–Asia project.

10 Author contribution

LC, YG and MZ conducted the study design. LC, JZ, HL, JL, KH, BG, XW, YL, CL, SI, TN, MK and KY contributed to modeling data. JF, ZW and JK provided the emission data and observation data. YG and JZ helped with data processing. MZ, JF and JZ were involved in the scientific interpretation and discussion. LC prepared the manuscript with contributions from all co-authors.

15 Competing interests

The authors declare that they have no conflict of interest.

Acknowledgements

This study was supported by the National Key R&D Programs of China (No. 2017YFC0209803), the National Natural Science Foundation of China (91544221, 91644215), the University Natural Science Research Foundation of Jiangsu Province (18KJB170012), the Startup Foundation for Introducing Talent of NUIST (2018r007) and the Decision-making Consultation Research Foundation of RICEG, NUIST (2018B33). Monthly pollution concentrations at EANET stations can be collected from <http://www.eanet.asia>. The AERONET Level 2.0 AOD data is downloaded from <https://aeronet.gsfc.nasa.gov/>. The MODIS and MISR AOD data are available at <https://ladsweb.modaps.eosdis.nasa.gov/> and <https://eosweb.larc.nasa.gov/>, respectively. Simulation results from the fourteen participating models to generate figures and tables in this manuscript have been archived by corresponding authors, and are available at <https://pan.baidu.com/s/1IaaCDhrAR-z2tO6yQNz2cg>.



References

- Ackermann, I. J., Hass, H., Memmesheimer, M., Ebel, A., Binkowski, F. S., and Shankar, U. M. A.: Modal aerosol dynamics model for Europe: Development and first applications. *Atmospheric environment*, 32(17), 2981-2999, 10.1016/S1352-2310(98)00006-5, 1998.
- 5 Alexander, B.: Sulfate formation in sea-salt aerosols: Constraints from oxygen isotopes, *Journal of Geophysical Research*, 110, 10.1029/2004jd005659, 2005.
- Baklanov, A., Schlünzen, K., Suppan, P., Baldasano, J., Brunner, D., Aksoyoglu, S., Carmichael, G., Douros, J., Flemming, J., Forkel, R., Galmarini, S., Gauss, M., Grell, G., Hirtl, M., Joffre, S., Jorba, O., Kaas, E., Kaasik, M., Kallos, G., Kong, X., Korsholm, U., Kurganskiy, A., Kushta, J., Lohmann, U., Mahura, A., Manders-Groot, A., Maurizi, A., Moussiopoulos, N., Rao, S. T., Savage, N., Seigneur, C., Sokhi, R. S., Solazzo, E., Solomos, S., Sørensen, B., Tsegas, G., Vignati, E., Vogel, B., and Zhang, Y.: Online coupled regional meteorology chemistry models in Europe: current status and prospects, *Atmos. Chem. Phys.*, 14, 317–398, <https://doi.org/10.5194/acp-14-317-2014>, 2014.
- 10 Bey, I., Jacob, D. J., Yantosca, R. M., Logan, J. A., Field, B. D., Fiore, A. M., Li, Q., Liu, H. Y., Mickley, L. J., and Schultz, M. G.: Global modeling of tropospheric chemistry with assimilated meteorology: Model description and evaluation, *Journal of Geophysical Research: Atmospheres*, 106, 23073-23095, 10.1029/2001jd000807, 2001.
- 15 Briant, R., Tuccella, P., Deroubaix, A., Khvorostyanov, D., Menut, L., Mailler, S., and Turquety, S.: Aerosol–radiation interaction modelling using online coupling between the WRF 3.7.1 meteorological model and the CHIMERE 2016 chemistry-transport model, through the OASIS3-MCT coupler, *Geoscientific Model Development*, 10, 927-944, 10.5194/gmd-10-927-2017, 2017.
- 20 Brunner, D., Savage, N., Jorba, O., Eder, B., Giordano, L., Badia, A., Balzarini, A., Baró R., Bianconi, R., Chemel, C., Curci, G., Forkel, R., Jiménez-Guerrero, P., Hirtl, M., Hodzic, A., Honzak, L., Im, U., Knote, C., Makar, P., Manders-Groot, A., van Meijgaard, E., Neal, L., Pérez, J. L., Pirovano, G., San Jose, R., Schröder, W., Sokhi, R. S., Syrakov, D., Torian, A., Tuccella, P., Werhahn, J., Wolke, R., Yahya, K., Zabkar, R., Zhang, Y., Hogrefe, C., and Galmarini, S.: Comparative analysis of meteorological performance of coupled chemistry-meteorology models in the context of AQMEII phase 2, *Atmospheric Environment*, 115, 470-498, 10.1016/j.atmosenv.2014.12.032, 2015.
- 25 Byun, D. W. and Ching, J. K. S.: Science algorithms of the EPA Models-3 Community Multiscale Air Quality (CMAQ) modeling system, US Environmental Protection Agency Report EPA/600/R-99/030, Research Triangle Park, NC, 1999.
- Carmichael, G. R., Calori, G., Hayami, H., Uno, I., Cho, S. Y., Engardt, M., Kim, S., Ichikawa, Y., Ikeda, Y., Ueda, H., Amann, M.: The MICS-Asia study: model intercomparison of long-range transport and sulfur deposition in East Asia. *Atmospheric Environment*, 36(2), 175-199, 10.1023/A:1012291200633, 2002.
- 30 Carmichael, G., Sakurai, T., Streets, D., Hozumi, Y., Ueda, H., Park, S., Fung, C., Han, Z., Kajino, M., and Engardt, M.: MICS-Asia II: The model intercomparison study for Asia Phase II methodology and overview of findings, *Atmospheric Environment*, 42, 3468-3490, 10.1016/j.atmosenv.2007.04.007, 2008.
- Carmichael, G. R., Adhikary, B., Kulkarni, S., D’Allura, A., Tang, Y., Streets, D., Zhang, Q., Bond, T. C., Ramanathan, V., Jamroensan, A., and Marrapu, P.: Asian Aerosols: Current and Year 2030 Distributions and Implications to Human Health and Regional Climate Change, *Environmental Science & Technology*, 43, 5811-5817, 10.1021/es8036803, 2009.
- 35 Carter, W. P. L.: Documentation of the SAPRC-99 chemical mechanism for VOC reactivity assessment. Final Report to California Air Resources Board Contract 92-329 and Contract 95-308, Air Pollution Research Center and College of Engineering Center for Environmental Research and Technology, University of California Riverside, California, 2000
- 40 Chen, D., Wang, Y., McElroy, M. B., He, K., Yantosca, R. M., and Sager, P. L.: Regional CO pollution and export in China simulated by the high-resolution nested-grid GEOS-Chem model. *Atmospheric Chemistry and Physics*, 9(11), 3825-3839, 10.5194/acp-9-3825-2009, 2009.
- Chen, K., Huang, L., Zhou, L., Ma, Z., Bi, J., and Li, T.: Spatial analysis of the effect of the 2010 heat wave on stroke mortality in Nanjing, China, *Sci Rep*, 5, 10816, 10.1038/srep10816, 2015.
- 45 Chen, L., Zhang, L., Zhang, L., Cao, X., Huang, J., Zhang, W., and Zhang, B.: Characteristics of black carbon aerosol and carbonaceous gases and their emission sources in semi-arid region, *China Environmental Science*, 32(8), 1345-1352, 2012.
- Chen, L., Zhang, M., and Wang, Y.: Model analysis of urbanization impacts on boundary layer meteorology under hot weather conditions: a case study of Nanjing, China, *Theoretical and Applied Climatology*, 125, 713-728,



- 10.1007/s00704-015-1535-6, 2016.
- Chen, L., Zhang, M., Zhu, J., and Skorokhod, A.: Model analysis of soil dust impacts on the boundary layer meteorology and air quality over East Asia in April 2015, *Atmospheric Research*, 187, 42-56, 10.1016/j.atmosres.2016.12.008, 2017.
- 5 Chen, L., Zhang, M. G., Zhu, J., Wang, Y. W., Skorokhod, A.: Modeling impacts of urbanization and urban heat island mitigation on boundary layer meteorology and air quality in Beijing under different weather conditions, *Journal of Geophysical Research: Atmospheres*, 123, doi: 10.1002/2017JD027501, 2018.
- Chin, M., Rood, R. B., Lin, S.-J., Müller, J.-F., and Thompson, A. M.: Atmospheric sulfur cycle simulated in the global model GOCART: Model description and global properties, *Journal of Geophysical Research: Atmospheres*, 105, 24671-24687, 10.1029/2000jd900384, 2000.
- 10 Chin, M., Ginoux, P., Kinne, S., Torres, O., Holben, B. N., Duncan, B. N., Martin, R. V., Logan, J. A., Higurashi, A., and Nakajima, T.: Tropospheric aerosol optical thickness from the GOCART model and comparisons with satellite and Sun photometer measurements, *J. Atmos. Sci.*, 59, 461-483, 10.1175/1520-0469(2002)059<0461:taotft>2.0.co;2, 2002.
- Cowan, T., Cai, W., Purich, A., Rotstayn, L., and England, M. H.: Forcing of anthropogenic aerosols on temperature trends of the sub-thermocline southern Indian Ocean, *Sci Rep*, 3, 2245, 10.1038/srep02245, 2013.
- 15 Cuchiara, G. C., Li, X., Carvalho, J., and Rappenglück, B.: Intercomparison of planetary boundary layer parameterization and its impacts on surface ozone concentration in the WRF/Chem model for a case study in Houston/Texas, *Atmospheric Environment*, 96, 175-185, 10.1016/j.atmosenv.2014.07.013, 2014.
- Deng, X. L., Shi, C. E., Wu, B. W., Yang, Y. J., Jin, Q., Wang, H. L., Zhu, S., and Yu, C.: Characteristics of the water-soluble components of aerosol particles in Hefei, China, *Journal of environmental sciences*, 42, 32-40, 10.1016/j.jes.2015.07.010, 2016.
- 20 Diehl, T., Heil, A., Chin, M., Pan, X., Streets, D., Schultz, M., and Kinne, S.: Anthropogenic, biomass burning, and volcanic emissions of black carbon, organic carbon, and SO₂ from 1980 to 2010 for hindcast model experiments, *Atmospheric Chemistry and Physics Discussions*, 12, 24895-24954, 10.5194/acpd-12-24895-2012, 2012.
- Ding, A. J., Huang, X., Nie, W., Sun, J. N., Kerminen, V. M., Petäjä T., Su, H., Cheng, Y. F., Yang, X. Q., Wang, M. H., Chi, X. G., Wang, J. P., Virkkula, A., Guo, W. D., Yuan, J., Wang, S. Y., Zhang, R. J., Wu, Y. F., Song, Y., Zhu, T., Zilitinkevich, S., Kulmala, M., and Fu, C. B.: Enhanced haze pollution by black carbon in megacities in China, *Geophysical Research Letters*, 43, 2873-2879, 10.1002/2016gl067745, 2016.
- Duncan Fairlie, T., Jacob, D. J., and Park, R. J.: The impact of transpacific transport of mineral dust in the United States, *Atmospheric Environment*, 41, 1251-1266, 10.1016/j.atmosenv.2006.09.048, 2007.
- 30 Easter, R. C.: MIRAGE: Model description and evaluation of aerosols and trace gases, *Journal of Geophysical Research*, 109, 10.1029/2004jd004571, 2004.
- Fan, Q., Lan, J., Liu, Y., Wang, X., Chan, P., Hong, Y., Feng, Y., Liu, Y., Zeng, Y., and Liang, G.: Process analysis of regional aerosol pollution during spring in the Pearl River Delta region, China, *Atmospheric Environment*, 122, 829-838, 10.1016/j.atmosenv.2015.09.013, 2015.
- 35 Fountoukis, C. and Nenes, A.: ISORROPIA II: a computationally efficient thermodynamic equilibrium model for K⁺-Ca²⁺-Mg²⁺-NH₄⁺-Na⁺-SO₄²⁻-NO₃⁻-Cl⁻-H₂O aerosols, *Atmos. Chem. Physics*, 7, 4639-4659, doi:10.5194/acp-7-4639-2007, <http://www.atmos-chem-phys.net/7/4639/2007/>, 2007.
- Forkel, R., Balzarini, A., Baro, R., Curci, C., Jimenez-Guerrero, P., Hirtl, J., Honzak, L., Im, U., Lorenz, C., Perez, J. L., Provano, G., San Jose, R., Tuccella, P., Werhahn, I., and Zabkar, R.: Analysis of the WRF-Chem contributions to AQMEII phase 2 with respect to aerosol radiative feedbacks on meteorology and pollutant distribution, *Atmospheric Environment*, 115, 630-645, doi: 10.1016/j.atmosenv.2014.10.056, 2015.
- 40 Fu, J., Jang, C., Streets, D., Li, Z., Kwok, R., Park, R., and Han, Z.: MICS-Asia II: Modeling gaseous pollutants and evaluating an advanced modeling system over East Asia, *Atmospheric Environment*, 42, 3571-3583, 10.1016/j.atmosenv.2007.07.058, 2008.
- 45 Fu, J. S., Hsu, N. C., Gao, Y., Huang, K., Li, C., Lin, N. H., and Tsay, S. C.: Evaluating the influences of biomass burning during 2006 BASE-ASIA: a regional chemical transport modeling, *Atmospheric Chemistry and Physics*, 12, 3837-3855, 10.5194/acp-12-3837-2012, 2012.
- Gao, M., Guttikunda, S. K., Carmichael, G. R., Wang, Y., Liu, Z., Stanier, C. O., Saide, P. E., and Yu, M.: Health impacts and economic losses assessment of the 2013 severe haze event in Beijing area, *Sci Total Environ*, 511, 553-561, 10.1016/j.scitotenv.2015.01.005, 2015a.
- 50



- Gao, M., Carmichael, G. R., Wang, Y., Saide, P. E., Yu, M., Xin, J., Liu, Z., and Wang, Z.: Modeling study of the 2010 regional haze event in the North China Plain, *Atmospheric Chemistry and Physics*, 16, 1673-1691, 10.5194/acp-16-1673-2016, 2016b.
- 5 Gao, M., Han, Z., Liu, Z., Li, M., Xin, J., Tao, Z., Li, J., Kang, J.-E., Huang, K., Dong, X., Zhuang, B., Li, S., Ge, B., Wu, Q., Cheng, Y., Wang, Y., Lee, H.-J., Kim, C.-H., Fu, J. S., Wang, T., Chin, M., Woo, J.-H., Zhang, Q., Wang, Z., and Carmichael, G. R.: Air Quality and Climate Change, Topic 3 of the Model Inter-Comparison Study for Asia Phase III (MICS-Asia III), Part I: overview and model evaluation, *Atmospheric Chemistry and Physics*, 18, 4859-4884, doi: 10.5194/acp-18-4859-2018, 2018.
- 10 Gao, Y., Zhao, C., Liu, X., Zhang, M., and Leung, L. R.: WRF-Chem simulations of aerosols and anthropogenic aerosol radiative forcing in East Asia, *Atmospheric Environment*, 92, 250-266, 10.1016/j.atmosenv.2014.04.038, 2014.
- Gao, Y., Zhang, M., Liu, Z., Wang, L., Wang, P., Xia, X., Tao, M., and Zhu, L.: Modeling the feedback between aerosol and meteorological variables in the atmospheric boundary layer during a severe fog-haze event over the North China Plain, *Atmospheric Chemistry and Physics*, 15, 4279-4295, 10.5194/acp-15-4279-2015, 2015b.
- 15 Gao, Y., Zhang, M., Liu, X., and Wang, L.: Change in diurnal variations of meteorological variables induced by anthropogenic aerosols over the North China Plain in summer 2008, *Theoretical and applied climatology*, 124(1-2), 103-118, 10.1007/s00704-015-1403-4, 2016a.
- Grell, G. A., Peckham, S. E., Schmitz, R., McKeen, S. A., Frost, G., Skamarock, W. C., and Eder, B.: Fully coupled “online” chemistry within the WRF model, *Atmospheric Environment*, 39, 6957-6975, 10.1016/j.atmosenv.2005.04.027, 2005.
- 20 Guenther, C. C.: Estimates of global terrestrial isoprene emissions using MEGAN (Model of Emissions of Gases and Aerosols from Nature). *Atmospheric Chemistry and Physics*, 6, www.atmos-chem-phys.net/6/3181/2006, 2006.
- Hall, D.: Environmental change, protest, and havens of environmental degradation: Evidence from Asia. *Global Environmental Politics*, 2(2), 20-28, 10.1162/15263800260047808, 2002.
- Han, X., Zhang, M., Liu, X., Steven, G., Xin, J., Wang, L.: Development of RAMS-CMAQ to simulate aerosol optical depth and aerosol direct radiative forcing and its application to East Asia. *Atmospheric and Oceanic Science Letters*, 2(6), 368-375, 10.1080/16742834.2009.11446831, 2009.
- 25 Han, X., Zhang, M., Tao, J., Wang, L., Gao, J., Wang, S., and Chai, F.: Modeling aerosol impacts on atmospheric visibility in Beijing with RAMS-CMAQ, *Atmospheric Environment*, 72, 177-191, 10.1016/j.atmosenv.2013.02.030, 2013.
- Han, X., Zhang, M., Gao, J., Wang, S., and Chai, F.: Modeling analysis of the seasonal characteristics of haze formation in Beijing, *Atmospheric Chemistry and Physics*, 14, 10231-10248, 10.5194/acp-14-10231-2014, 2014.
- 30 Han, X., Zhu, L., Wang, S., Meng, X., Zhang, M., and Hu, J.: Modeling study of impacts on surface ozone of regional transport and emissions reductions over North China Plain in summer 2015, *Atmospheric Chemistry and Physics*, 18, 12207-12221, 10.5194/acp-18-12207-2018, 2018.
- Han, Z., Sakurai, T., Ueda, H., Carmichael, G., Streets, D., Hayami, H., Wang, Z., Holloway, T., Engardt, M., and Hozumi, Y.: MICS-Asia II: Model intercomparison and evaluation of ozone and relevant species, *Atmospheric Environment*, 42, 3491-3509, 10.1016/j.atmosenv.2007.07.031, 2008.
- 35 Hauser, A., Oesch, D., and Foppa, N.: Aerosol optical depth over land: Comparing AERONET, AVHRR and MODIS, *Geophysical Research Letters*, 32, 10.1029/2005gl023579, 2005.
- Hayami, H., Sakurai, T., Han, Z., Ueda, H., Carmichael, G., Streets, D., Holloway, T., Wang, Z., Thongboonchoo, N., and Engardt, M.: MICS-Asia II: Model intercomparison and evaluation of particulate sulfate, nitrate and ammonium, *Atmospheric Environment*, 42, 3510-3527, 10.1016/j.atmosenv.2007.08.057, 2008.
- 40 Holben, B. N., Eck, T. F., Slutsker, I., Tanre, D., Buis, J. P., Setzer, A., Vermote, E., Reagan, J. A., Kaufman, Y. J., Nakajima, T., Lavenu, F., Jankowiak, I., Smirnov, A.: AERONET—A federated instrument network and data archive for aerosol characterization. *Remote sensing of environment*, 66(1), 1-16, 10.1016/S0034-4257(98)00031-5, 1998.
- Holloway, T., Sakurai, T., Han, Z., Ehlers, S., Spak, S., Horowitz, L., Carmichael, G., Streets, D., Hozumi, Y., and Ueda, H.: MICS-Asia II: Impact of global emissions on regional air quality in Asia, *Atmospheric Environment*, 42, 3543-3561, 10.1016/j.atmosenv.2007.10.022, 2008.
- 45 Hong, C., Zhang, Q., He, K., Guan, D., Li, M., Liu, F., and Zheng, B.: Variations of China's emission estimates: response to uncertainties in energy statistics, *Atmospheric Chemistry and Physics*, 17, 1227-1239, 10.5194/acp-17-1227-2017, 2017.
- 50 Horowitz, L. W., Walters, S., Mauzerall, D. L., Emmons, L. K., Rasch, P. J., Granier, C., Tie, X. X., Lamarque, J. F., Schultz,



- M. G., Tyndall, G. S., Orlando, J. J., and Brasseur, G. P.: A global simulation of tropospheric ozone and related tracers: Description and evaluation of MOZART, version 2, *J. Geophys. Res.-Atmos.*, 108, 29, 10.1029/2002jd002853, 2003.
- Huang, K., Fu, J. S., Hsu, N. C., Gao, Y., Dong, X., Tsay, S.-C., and Lam, Y. F.: Impact assessment of biomass burning on air quality in Southeast and East Asia during BASE-ASIA, *Atmospheric Environment*, 78, 291-302, 10.1016/j.atmosenv.2012.03.048, 2013.
- 5 Huang, X., Song, Y., Li, M., Li, J., Huo, Q., Cai, X., Zhu, T., Hu, M., and Zhang, H.: A high-resolution ammonia emission inventory in China, *Global Biogeochem. Cy.*, 26, GB1030, doi:10.1029/2011GB004161, 2012.
- Huang, X., Song, Y., Zhao, C., Li, M., Zhu, T., Zhang, Q., and Zhang, X.: Pathways of sulfate enhancement by natural and anthropogenic mineral aerosols in China, *J. Geophys. Res.-Atmos.*, 119, <https://doi.org/10.1002/2014JD022301>, 2014.
- 10 Huang, X., Wang, Z., and Ding, A.: Impact of Aerosol-PBL Interaction on Haze Pollution: Multiyear Observational Evidences in North China, *Geophysical Research Letters*, 10.1029/2018gl079239, 2018.
- Ikeda, K., Yamaji, K., Kanaya, Y., Taketani, F., Pan, X., Komazaki, Y., Kurokawa, J.-i., and Ohara, T.: Sensitivity analysis of source regions to PM_{2.5} concentration at Fukue Island, Japan, *Journal of the Air & Waste Management Association*, 64, 445-452, 10.1080/10962247.2013.845618, 2013.
- 15 Itahashi, S., Uno, I., Irie, H., Kurokawa, J. I., and Ohara, T.: Regional modeling of tropospheric NO₂ vertical column density over East Asia during the period 2000–2010: comparison with multisatellite observations, *Atmospheric Chemistry and Physics*, 14, 3623-3635, 10.5194/acp-14-3623-2014, 2014.
- Janssens-Maenhout, G., Crippa, M., Guizzardi, D., Dentener, F., Muntean, M., Pouliot, G., Keating, T., Zhang, Q., Kurokawa, J., Wankmüller, R., Denier van der Gon, H., Kuenen, J. J. P., Klimont, Z., Frost, G., Darras, S., Koffi, B., and Li, M.: HTAP_v2.2: a mosaic of regional and global emission grid maps for 2008 and 2010 to study hemispheric transport of air pollution, *Atmospheric Chemistry and Physics*, 15, 11411-11432, 10.5194/acp-15-11411-2015, 2015.
- 20 Jongman, B., Winsemius, H. C., Aerts, J. C., Coughlan de Perez, E., van Aalst, M. K., Kron, W., and Ward, P. J.: Declining vulnerability to river floods and the global benefits of adaptation, *Proc Natl Acad Sci U S A*, 112, E2271-2280, 10.1073/pnas.1414439112, 2015.
- 25 Kajino, M., Inomata, Y., Sato, K., Ueda, H., Han, Z., An, J., Katata, G., Deushi, M., Maki, T., Oshima, N., Kurokawa, J., Ohara, T., Takami, A., and Hatakeyama, S.: Development of the RAQM2 aerosol chemical transport model and predictions of the Northeast Asian aerosol mass, size, chemistry, and mixing type. *Atmospheric Chemistry and Physics*, 12(24), 11833, 10.5194/acp-12-11833-2012, 2012.
- Kurokawa, J., Ohara, T., Morikawa, T., Hanayama, S., Janssens-Maenhout, G., Fukui, T., Kawashima, K., and Akimoto, H.: Emissions of air pollutants and greenhouse gases over Asian regions during 2000–2008: Regional Emission inventory in Asia (REAS) version 2, *Atmos. Chem. Phys.*, 13, 11019–11058, doi:10.5194/acp-13-11019-2013, 2013.
- 30 Kiley, C. M., Fuelberg, H. E., Palmer, P. I., Allen, D. J., Carmichael, G. R., Jacob, D. J., Mari, C., Pierce, R. B., Pickering, K. E., Tang, Y., Wild, O., Fairlie, T. D., Logan, J. A., Sachse, G. W., Shaack, T. K., and Streets, D. G.: An intercomparison and evaluation of aircraft-derived and simulated CO from seven chemical transport models during the TRACE-P experiment, *Journal of Geophysical Research: Atmospheres*, 108, 10.1029/2002jd003089, 2003.
- 35 Kim, Y. J., Spak, S. N., Carmichael, G. R., Riemer, N., and Stanier, C. O.: Modeled aerosol nitrate formation pathways during wintertime in the Great Lakes region of North America, *J. Geophys. Res. Atmos.*, 119, 12420–12445, 2014.
- Kong, X., Forkel, R., Sokhi, R. S., Suppan, P., Baklanov, A., Gauss, M., Brunner, D., Baro, R., Balzarini, A., Chemel, C., Curci, G., Jimenez-Guerrero, P., Hirtl, M., Honzak, L., Im, U., Perez, J. L., Pirovano, G., Jose, R. S., Schlunzen, K. H., Tsegas, G., Tuccella, P., Werhahn, J., Zabkar, R., and Galmarini, S.: Analysis of meteorology-chemistry interactions during air pollution episodes using online coupled models within AQMEII phase-2, 115, 527-540, doi: 10.1016/j.atmosenv.2014.09.020, 2015.
- 40 Lai, S., Zhao, Y., Ding, A., Zhang, Y., Song, T., Zheng, J., Ho, K. F., Lee, S.-c., and Zhong, L.: Characterization of PM_{2.5} and the major chemical components during a 1-year campaign in rural Guangzhou, Southern China, *Atmospheric Research*, 167, 208-215, 10.1016/j.atmosres.2015.08.007, 2016.
- 45 Lam, Y. F., Fu, J. S., Wu, S., and Mickley, L. J.: Impacts of future climate change and effects of biogenic emissions on surface ozone and particulate matter concentrations in the United States, *Atmospheric Chemistry and Physics*, 11, 4789-4806, 10.5194/acp-11-4789-2011, 2011.
- Lee, D. G., Lee, Y. M., Jang, K. W., Yoo, C., Kang, K. H., Lee, J. H., Jung, S. W., Park, J. M., Lee, S. B., Han, J. S., Hong, J. H., and Lee, S. J.: Korean national emissions inventory system and 2007 air pollutant emissions, *Asian J. Atmos.*
- 50



- Environ., 5, 278–291, 2011.
- Lee, H.-J., Jo, H.-Y., Nam, K.-P., Lee, K.-H., Kim, C.-H.: Measurement, simulation, and meteorological interpretation of medium-range transport of radionuclides to Korea during the Fukushima Dai-ichi nuclear accident, *Annals of Nuclear Energy*, 103, 412–423, doi: 10.1016/j.anucene.2017.01.037, 2017.
- 5 Li, B., Yuan, H., Feng, N., and Tao, S.: Comparing MODIS and AERONET aerosol optical depth over China, *International Journal of Remote Sensing*, 30, 6519–6529, 10.1080/01431160903111069, 2009.
- Li, J., Han, Z., and Zhang, R.: Model study of atmospheric particulates during dust storm period in March 2010 over East Asia, *Atmospheric Environment*, 45, 3954–3964, 10.1016/j.atmosenv.2011.04.068, 2011.
- 10 Li, J., Wang, Z., Zhuang, G., Luo, G., Sun, Y., and Wang, Q.: Mixing of Asian mineral dust with anthropogenic pollutants over East Asia: a model case study of a super-duststorm in March 2010, *Atmospheric Chemistry and Physics*, 12, 7591–7607, 10.5194/acp-12-7591-2012, 2012a.
- Li, J.: Research on pollution characteristics of PM₁₀ in Jinan and inversion of aerosol optical thickness, M.S. thesis, Shandong Normal University, China, 64 pp., 2012b.
- Li, J.: Seasonal characteristics of air pollution and weekend effect in Shanghai, M.S. thesis, the University of Chinese Academy of Sciences, China, 77 pp., 2015.
- 15 Li, J., Chen, X., Wang, Z., Du, H., Yang, W., Sun, Y., Hu, B., Li, J., Wang, W., Wang, T., Fu, P., and Huang, H.: Radiative and heterogeneous chemical effects of aerosols on ozone and inorganic aerosols over East Asia, *The Science of the total environment*, 622–623, 1327–1342, 10.1016/j.scitotenv.2017.12.041, 2018.
- Li, Y., An, J., and Gultepe, I.: Effects of additional HONO sources on visibility over the North China Plain, *Advances in Atmospheric Sciences*, 31, 1221–1232, 10.1007/s00376-014-4019-1, 2014.
- 20 Li, Y., Tao, J., Zhang, L., Jia, X., and Wu, Y.: High Contributions of Secondary Inorganic Aerosols to PM_{2.5} under Polluted Levels at a Regional Station in Northern China, *International journal of environmental research and public health*, 13, 10.3390/ijerph13121202, 2016a.
- Li, K., Liao, H., Zhu, J., and Moch, J. M.: Implications of RCP emissions on future PM_{2.5} air quality and direct radiative forcing over China, *Journal of Geophysical Research: Atmospheres*, 121, 12,985–913,008, 10.1002/2016jd025623, 2016b.
- Li, K., Liao, H., Mao, Y., and Ridley, D. A.: Source sector and region contributions to concentration and direct radiative forcing of black carbon in China, *Atmospheric Environment*, 124, 351–366, 10.1016/j.atmosenv.2015.06.014, 2016c.
- 30 Li, J., Du, H., Wang, Z., Sun, Y., Yang, W., Li, J., Tang, X., and Fu, P.: Rapid formation of a severe regional winter haze episode over a mega-city cluster on the North China Plain, *Environ Pollut*, 223, 605–615, 10.1016/j.envpol.2017.01.063, 2017a.
- Li, M., Zhang, Q., Kurokawa, J.-i., Woo, J.-H., He, K., Lu, Z., Ohara, T., Song, Y., Streets, D. G., Carmichael, G. R., Cheng, Y., Hong, C., Huo, H., Jiang, X., Kang, S., Liu, F., Su, H., and Zheng, B.: MIX: a mosaic Asian anthropogenic emission inventory under the international collaboration framework of the MICS-Asia and HTAP, *Atmospheric Chemistry and Physics*, 17, 935–963, 10.5194/acp-17-935-2017, 2017b.
- 35 Liao, H., Chen, W.-T., and Seinfeld, J. H.: Role of climate change in global predictions of future tropospheric ozone and aerosols, *Journal of Geophysical Research*, 111, 10.1029/2005jd006852, 2006.
- Lin, C. Y., Zhao, C., Liu, X., Lin, N. H., and Chen, W. N.: Modelling of long-range transport of Southeast Asia biomass-burning aerosols to Taiwan and their radiative forcings over East Asia. *Tellus B: Chemical and Physical Meteorology*, 66(1), 23733, 10.3402/tellusb.v66.23733, 2014.
- 40 Liu, H., Jacob, D. J., Bey, I., and Yantosca, R. M.: Constraints from ²¹⁰Pb and ⁷Be on wet deposition and transport in a global three-dimensional chemical tracer model driven by assimilated meteorological fields, *Journal of Geophysical Research: Atmospheres*, 106, 12109–12128, 10.1029/2000jd900839, 2001.
- Liu, S.: Research of observations of haze and precursors in Tangshan industrial zone, M.S. thesis, Nanjing University of Information Science & Technology, China, 71 pp., 2012.
- 45 Liu, X. G., Li, J., Qu, Y., Han, T., Hou, L., Gu, J., Chen, C., Yang, Y., Liu, X., Yang, T., Zhang, Y., Tian, H., and Hu, M.: Formation and evolution mechanism of regional haze: a case study in the megacity Beijing, China, *Atmos. Chem. Phys.*, 13, 4501–4514, doi:10.5194/acp-13-4501-2013, 2013.
- Lohmann, U., and Diehl, K.: Sensitivity studies of the importance of dust ice nuclei for the indirect aerosol effect on stratiform mixed-phase clouds. *Journal of the Atmospheric Sciences*, 63(3), 968–982, 10.1175/JAS3662.1, 2006.
- 50



- Lu, Z., Zhang, Q., and Streets, D. G.: Sulfur dioxide and primary carbonaceous aerosol emissions in China and India, 1996–2010, *Atmos. Chem. Phys.*, 11, 9839–9864, doi:10.5194/acp-11-9839-2011, 2011.
- Meng, Z., Jia, X., Zhang, R., Yu, X., and Ma, Q.: Characteristics of PM_{2.5} at Lin'an regional background station in the Yangtze River Delta Region, *Journal of Applied Meteorological Science*, 23(4), 424–432, 2012.
- 5 Monahan, E. C. and Muirchearthaigh, I. O.: Optimal Power-Law Description of Oceanic Whitecap Coverage Dependence on Wind Speed, *J. Phys. Oceanogr.*, 10, 2094–2099, doi:10.1175/1520-0485(1980)010<2094:OPLDOO>2.0.CO;2, 1980.
- Nagashima, T., Sudo, K., Akimoto, H., Kurokawa, J., and Ohara T.: Long-term change in the source contribution to surface ozone over Japan, *Atmos. Chem. Phys.*, 17, 8231–8246, doi: 10.5194/acp-17-8231-2017, 2017.
- 10 Nenes, A., Pandis, S. N., and Pilinis, C.: ISORROPIA: A new thermodynamic equilibrium model for multiphase multicomponent inorganic aerosols. *Aquatic geochemistry*, 4(1), 123–152, 10.1023/A:1009604003981, 1998.
- Nolte, C. G., Gilliland, A. B., Hogrefe, C., and Mickley, L. J.: Linking global to regional models to assess future climate impacts on surface ozone levels in the United States, *Journal of Geophysical Research*, 113, 10.1029/2007jd008497, 2008.
- 15 Pan, Y., Tian, S., Liu, D., Fang, Y., Zhu, X., Zhang, Q., Zheng, B., Michalski, G., and Wang, Y.: Fossil fuel combustion-related emissions dominate atmospheric ammonia sources during severe haze episodes: evidence from ¹⁵N-Stable isotope in size-resolved aerosol ammonium, *Environ. Sci. Technol.*, 50(15), 8049–8056, 10.1021/acs.est.6b00634, 2016.
- Park, R. J.: Sources of carbonaceous aerosols over the United States and implications for natural visibility, *Journal of Geophysical Research*, 108, 10.1029/2002jd003190, 2003.
- 20 Park, R. J.: Natural and transboundary pollution influences on sulfate-nitrate-ammonium aerosols in the United States: Implications for policy, *Journal of Geophysical Research*, 109, 10.1029/2003jd004473, 2004.
- Petaja, T., Jarvi, L., Kerminen, V. M., Ding, A. J., Sun, J. N., Nie, W., Kujansuu, J., Virkkula, A., Yang, X. Q., Fu, C. B., Zilitinkevich, S., and Kulmala, M.: Enhanced air pollution via aerosol-boundary layer feedback in China, *Sci Rep*, 6, 18998, 10.1038/srep18998, 2016.
- 25 Phadnis, M. J., Carmichael, G. R., Ichikawa, Y., and Hayami, H.: Evaluation of long-range transport models for acidic deposition in East Asia. *Journal of Applied Meteorology*, 37(10), 1127–1142, 10.1175/1520-0450(1998)037<1127:EOLRTM>2.0.CO;2, 1998.
- Pleim, J. E., and Chang, J. S.: A non-local closure model for vertical mixing in the convective boundary layer. *Atmospheric Environment. Part A. General Topics*, 26(6), 965–981, 10.1016/0960-1686(92)90028-J, 1992.
- 30 Pleim, J. E., Xiu, A., Finkelstein, P. L., and Otte, T. L.: A coupled land-surface and dry deposition model and comparison to field measurements of surface heat, moisture, and ozone fluxes. *Water, Air, & Soil Pollution: Focus*, 1(5), 243–252, 10.1023/A:1013123725860, 2001.
- Pope, C. A., and Dockery, D. W.: Health Effects of Fine Particulate Air Pollution: Lines that Connect, *Journal of the Air & Waste Management Association*, 56, 709–742, 10.1080/10473289.2006.10464485, 2006.
- 35 Pye, H. O. T., Liao, H., Wu, S., Mickley, L. J., Jacob, D. J., Henze, D. K., and Seinfeld, J. H.: Effect of changes in climate and emissions on future sulfate-nitrate-ammonium aerosol levels in the United States, *Journal of Geophysical Research*, 114, 10.1029/2008jd010701, 2009.
- Qiu, Y., Liao, H., Zhang, R., and Hu, J.: Simulated impacts of direct radiative effects of scattering and absorbing aerosols on surface layer aerosol concentrations in China during a heavily polluted event in February 2014, *Journal of Geophysical Research: Atmospheres*, 122, 5955–5975, 10.1002/2016jd026309, 2017.
- 40 Tao, J., Zhang, L., Ho, K., Zhang, R., Lin, Z., Zhang, Z., Lin, M., Cao, J., Liu, S., and Wang, G.: Impact of PM_{2.5} chemical compositions on aerosol light scattering in Guangzhou — the largest megacity in South China, *Atmospheric Research*, 135–136, 48–58, 10.1016/j.atmosres.2013.08.015, 2014.
- Toth, T. D., Zhang, J., Campbell, J. R., Reid, J. S., Shi, Y., Johnson, R. S., Smirnov, A., Vaughan, M. A., and Winker, D. M.: Investigating enhanced Aqua MODIS aerosol optical depth retrievals over the mid-to-high latitude Southern Oceans through intercomparison with co-located CALIOP, MAN, and AERONET data sets, *Journal of Geophysical Research: Atmospheres*, 118, 4700–4714, 10.1002/jgrd.50311, 2013.
- 45 Reams, M. A., Lam, N. S., and Baker, A.: Measuring Capacity for Resilience among Coastal Counties of the US Northern Gulf of Mexico Region, *Am J Clim Change*, 1, 194–204, 10.4236/ajcc.2012.14016, 2012.
- 50 Schell, B., Ackermann, I. J., Hass, H., Binkowski, F. S., and Ebel, A.: Modeling the formation of secondary organic aerosol



- within a comprehensive air quality model system, *Journal of Geophysical Research: Atmospheres*, 106, 28275-28293, 10.1029/2001jd000384, 2001.
- Seinfeld, J. H. and Pandis, S. N.: *Atmospheric chemistry and physics: from air pollution to climate change*, John Wiley & Sons, USA New Jersey John Wiley & Sons, INC, 2016.
- 5 Shao, P.: *The network observation and research on air pollution in Zhangjiakou, Beijing and Langfang*, M.S. thesis, Nanjing University of Information Science & Technology, China, 66 pp., 2012.
- Shimadera, H., Hayami, H., Chatani, S., Morino, Y., Mori, Y., Morikawa, T., Yamaji, K., and Ohara, T.: Sensitivity analyses of factors influencing CMAQ performance for fine particulate nitrate, *Journal of the Air & Waste Management Association*, 64, 374-387, 10.1080/10962247.2013.778919, 2013.
- 10 Singh, A., and Dey, S.: Influence of aerosol composition on visibility in megacity Delhi, *Atmospheric Environment*, 62, 367-373, 10.1016/j.atmosenv.2012.08.048, 2012.
- Spence, M., Clarke, A., Buckley, R.M.: *Urbanization and Growth; Commission on Growth and Development*, World Bank Publications: Washington, DC, USA, 2008.
- Stockwell, W. R., Middleton, P., Chang, J. S., and Tang, X.: The second generation regional acid deposition model chemical mechanism for regional air quality modeling. *Journal of Geophysical Research: Atmospheres*, 95(D10), 16343-16367, 10.1029/JD095iD10p16343, 1990.
- 15 Stockwell, W. R., Kirchner, F., Kuhn, M., and Seefeld, S.: A new mechanism for regional atmospheric chemistry modeling, *Journal of Geophysical Research: Atmospheres*, 102, 25847-25879, 10.1029/97jd00849, 1997.
- Stuefer, M., Freitas, S. R., Grell, G., Webley, P., Peckham, S., McKeen, S. A., and Egan, S. D.: Inclusion of ash and SO₂ emissions from volcanic eruptions in WRF-Chem: development and some applications. *Geoscientific Model Development*, 6(2), 457-468, 10.5194/gmd-6-457-2013, 2013.
- 20 Su, X., Tie, X., Li, G., Cao, J., Huang, R., Feng, T., Long, X., and Xu, R.: Effect of hydrolysis of N₂O₅ on nitrate and ammonium formation in Beijing China: WRF-Chem model simulation, *The Science of the total environment*, 579, 221-229, 10.1016/j.scitotenv.2016.11.125, 2017.
- 25 Sudo, K., Takahashi, M., Kurokawa, J., and Akimoto, H.: CHASER: A global chemical model of the troposphere-1. Model description, *J. Geophys. Res.-Atmos.*, 107, 20, 10.1029/2001jd001113, 2002a.
- Sudo, K., Takahashi, M., and Akimoto, H.: CHASER: A global chemical model of the troposphere-2. Model results and evaluation, *J. Geophys. Res.-Atmos.*, 107, 39, 10.1029/2001jd001114, 2002b.
- Sun, Y. L., Wang, Z. F., Du, W., Zhang, Q., Wang, Q. Q., Fu, P. Q., Pan, X. L., Li, J., Jayne, J., and Worsnop, D. R.: Long-term real-time measurements of aerosol particle composition in Beijing, China: seasonal variations, meteorological effects, and source analysis, *Atmospheric Chemistry and Physics*, 15, 10149-10165, 10.5194/acp-15-10149-2015, 2015.
- 30 Sun, Y., Du, W., Fu, P., Wang, Q., Li, J., Ge, X., Zhang, Q., Zhu, C., Ren, L., Xu, W., Zhao, J., Han, T., Worsnop, D. R., and Wang, Z.: Primary and secondary aerosols in Beijing in winter: sources, variations and process, *Atmos. Chem. Phys.*, 16, 8309-8329, doi: 10.5194/acp-16-8309-2016, 2016.
- 35 Tuccella, P., Curci, G., Grell, G. A., Visconti, G., Crumeyrolle, S., Schwarzenboeck, A., and Mensah, A. A.: A new chemistry option in WRF-Chem v. 3.4 for the simulation of direct and indirect aerosol effects using VBS: evaluation against IMPACT-EUCAARI data, *Geoscientific Model Development*, 8, 2749-2776, 10.5194/gmd-8-2749-2015, 2015.
- van der Werf, G. R., Randerson, J. T., Giglio, L., Collatz, G. J., Mu, M., Kasibhatla, P. S., Morton, D. C., DeFries, R. S., Jin, Y., and van Leeuwen, T. T.: Global fire emissions and the contribution of deforestation, savanna, forest, agricultural, and peat fires (1997-2009). *Atmos. Chem. Phys.*, 10, 11707-11753, 10.5194/acp-10-11707-2010, 2010.
- 40 Walcek, C. J., and Taylor, G. R.: A theoretical method for computing vertical distributions of acidity and sulfate production within cumulus clouds. *Journal of the Atmospheric Sciences*, 43(4), 339-355, 10.1175/1520-0469(1986)043<0339:ATMFCV>2.0.CO;2, 1986.
- 45 Wang, C.: Impact of anthropogenic absorbing aerosols on clouds and precipitation: A review of recent progresses, *Atmospheric Research*, 122, 237-249, 10.1016/j.atmosres.2012.11.005, 2013a.
- Wang, H., He, Q., Chen, Y., and Kang, Y.: Analysis of Characteristics of Black Carbon Concentration in Shanghai from 2008 to 2012, *Environmental Science*, 35(4), 1215-1222, 2014a.
- 50 Wang, H., Xie, S.-P., and Liu, Q.: Comparison of Climate Response to Anthropogenic Aerosol versus Greenhouse Gas Forcing: Distinct Patterns, *Journal of Climate*, 29, 5175-5188, 10.1175/jcli-d-16-0106.1, 2016a.



- Wang, H. L., Qiao, L. P., Lou, S. R., Zhou, M., Ding, A. J., Huang, H. Y., Chen, J. M., Wang, Q., Tao, S. K., Chen, C. H., Li, L., and Huang, C.: Chemical composition of PM_{2.5} and meteorological impact among three years in urban Shanghai, China, *Journal of Cleaner Production*, 112, 1302-1311, 10.1016/j.jclepro.2015.04.099, 2016b.
- Wang, J., Wang, X., Zhang, H., Lu, F., and Hou, P.: Comparison of PM_{2.5} concentration and elemental compositions in two typical sites in Beijing urban area, *Acta Scientiae Circumstantiae*, 32(1), 74-80, 2012a.
- Wang, K., Zhang, Y., Nenes, A., and Fountoukis, C.: Implementation of dust emission and chemistry into the Community Multiscale Air Quality modeling system and initial application to an Asian dust storm episode, *Atmospheric Chemistry and Physics*, 12, 10209-10237, 2012b.
- Wang, P., Cao, J.-j., Shen, Z.-x., Han, Y.-m., Lee, S.-c., Huang, Y., Zhu, C.-s., Wang, Q.-y., Xu, H.-m., and Huang, R.-j.: Spatial and seasonal variations of PM 2.5 mass and species during 2010 in Xi'an, China, *Science of The Total Environment*, 508, 477-487, 10.1016/j.scitotenv.2014.11.007, 2015.
- Wang, P., Wang, H., Wang, Y. Q., Zhang, X. Y., Gong, S. L., Xue, M., Zhou, C. H., Liu, H. L., An, X. Q., Niu, T., and Cheng, Y. L.: Inverse modeling of black carbon emissions over China using ensemble data assimilation, *Atmospheric Chemistry and Physics*, 16, 989-1002, 10.5194/acp-16-989-2016, 2016c.
- Wang, X., Liao, J.B., Zhang, J., Shen, C., Chen, W.H., Xia, B.C. and Wang, T.J.: A Numeric Study of Regional Climate Change Induced by Urban Expansion in the Pearl River Delta, China, *J. Appl. Meteor. Climatol.*, 53, 346-362, doi: 10.1175/JAMC-D-13-054.1, 2014b.
- Wang, Y., Zhang, Q., He, K., Zhang, Q., and Chai, L.: Sulfate-nitrate-ammonium aerosols over China: response to 2000-2015 emission changes of sulfate dioxide, nitrogen oxides, and ammonia, *Atmos. Chem. Phys.*, 13, 2635-2652, doi: 10.5194/acp-13-2635-2013, 2013b.
- Wang, Z., Xie, F., Sakurai, T., Ueda, H., Han, Z., Carmichael, G., Streets, D., Engardt, M., Holloway, T., and Hayami, H.: MICS-Asia II: Model inter-comparison and evaluation of acid deposition, *Atmospheric Environment*, 42, 3528-3542, 10.1016/j.atmosenv.2007.12.071, 2008.
- Wang, Z., Maeda, T., Hayashi, M., Hsiao, L. F., and Liu, K. Y.: A nested air quality prediction modeling system for urban and regional scales: Application for high-ozone episode in Taiwan. *Water, Air, & Soil Pollution*, 130(1), 391-396, 10.1023/A:1013833217916, 2001.
- Wang, Z., Li, J., Wang, Z., Yang, W., Tang, X., Ge, B., Yan, P., Zhu, L., Chen, X., Chen, H., Wand, W., Li, J., Liu, B., Wang, X., Wand, W., Zhao, Y., Lu, N., and Su, D.: Modeling study of regional severe hazes over mid-eastern China in January 2013 and its implications on pollution prevention and control, *Science China Earth Sciences*, 57, 3-13, 10.1007/s11430-013-4793-0, 2013c.
- Wesely, M. L.: Parameterization of surface resistances to gaseous dry deposition in regional-scale numerical models. *Atmospheric Environment* (1967), 23(6), 1293-1304, 10.1016/0004-6981(89)90153-4, 1989.
- Xie, H., Wu, D., Zhang, G., Li, M., Fang, H., Chen, Q., Li, X., and Zhai, G.: Characteristic analysis of fine particles PM_{2.5} in the ambient air in Dongguan, *Air Pollution Control*, doi:10.13205/j.hjgc.201406016, 2013.
- Xu, Y.: The level of haze and PM_{2.5} in Zhengzhou and heat power plants' atmospheric environmental impact assessment, M.S. thesis, Zhengzhou University, China, 77 pp., 2012.
- Yamaji, K., Ohara, T., Uno, I., Kurokawa, J.-i., Pochanart, P., and Akimoto, H.: Future prediction of surface ozone over east Asia using Models-3 Community Multiscale Air Quality Modeling System and Regional Emission Inventory in Asia, *Journal of Geophysical Research*, 113, 10.1029/2007jd008663, 2008.
- Yan, Z.-W., Wang, J., Xia, J.-J., and Feng, J.-M.: Review of recent studies of the climatic effects of urbanization in China, *Advances in Climate Change Research*, 7, 154-168, 10.1016/j.accre.2016.09.003, 2016.
- Yao, L., Yang, L., Yuan, Q., Yan, C., Dong, C., Meng, C., Sui, X., Yang, F., Lu, Y., and Wang, W.: Sources apportionment of PM_{2.5} in a background site in the North China Plain, *The Science of the total environment*, 541, 590-598, 10.1016/j.scitotenv.2015.09.123, 2016.
- Yarwood, G., Rao, S., Yocke, M., and Whitten, G. Z.: Updates to the Carbon Bond Chemical Mechanism: CB05. Final Report to the US EPA, RT-0400675, 2005.
- Yu, Y., Hu, B., and Wang, Y.: Changing characteristics of the main air pollutants of the Dongling Mountain in Beijing, *Environmental Science*, 34(7), doi:10.13227/j.hjlx.2013.07.021, 2013.
- Yue, X., Unger, N., Harper, K., Xia, X., Liao, H., Zhu, T., Xiao, J., Feng, Z., and Li, J.: Ozone and haze pollution weakens net primary productivity in China, *Atmospheric Chemistry and Physics*, 17, 6073-6089, 10.5194/acp-17-6073-2017,



- 2017.
- Zaveri, R. A., and Peters, L. K.: A new lumped structure photochemical mechanism for large-scale applications, *Journal of Geophysical Research: Atmospheres*, 104, 30387-30415, 10.1029/1999jd900876, 1999.
- 5 Zhang, B., Wang, Y., and Hao, J.: Simulating aerosol–radiation–cloud feedbacks on meteorology and air quality over eastern China under severe haze condition in winter, *Atmospheric Chemistry and Physics*, 15, 2387-2404, 10.5194/acp-15-2387-2015, 2015a.
- Zhang, L., Gong, S., Padro, J., and Barrie, L.: A size-segregated particle dry deposition scheme for an atmospheric aerosol module. *Atmospheric Environment*, 35(3), 549-560, 10.1016/S1352-2310(00)00326-5, 2001.
- 10 Zhang, L., Chen, Y., Zhao Y., Henze, D., Zhu, L., Song, Y., Paulot, F., Liu, X., Pan, Y., Lin, Y., and Huang B.: Agricultural ammonia emissions in China: Reconciling bottom-up and top-down estimates, *Atmospheric Chemistry and Physics*, 18, 339-355, 10.5194/acp-18-339-2018, 2018.
- Zhang, M.: Numerical study of boundary layer ozone transport and photochemical production in east Asia in the wintertime, *Geophysical Research Letters*, 29, 10.1029/2001gl014368, 2002.
- 15 Zhang, M., Uno, I., Zhang, R., Han, Z., Wang, Z., and Pu, Y.: Evaluation of the Models-3 Community Multi-scale Air Quality (CMAQ) modeling system with observations obtained during the TRACE-P experiment: Comparison of ozone and its related species, *Atmospheric Environment*, 40, 4874-4882, 10.1016/j.atmosenv.2005.06.063, 2006.
- Zhang, M., Han, Z., and Zhu, L.: Simulation of atmospheric aerosols in East Asia using modeling system RAMS-CMAQ: Model evaluation, *China Particology*, 5, 321-327, 10.1016/j.cpart.2007.07.002, 2007.
- 20 Zhang, X.: Study on long-term variation of Black Carbon aerosol over Peking and Hebei province during 2006-2012, M.S. thesis, Yunnan University, China, 116 pp., 2015b.
- Zhao, P. S., Dong, F., He, D., Zhao, X. J., Zhang, X. L., Zhang, W. Z., Yao, Q., and Liu, H. Y.: Characteristics of concentrations and chemical compositions for PM_{3.5} in the region of Beijing, Tianjin, and Hebei, China, *Atmospheric Chemistry and Physics*, 13, 4631-4644, 10.5194/acp-13-4631-2012, 2013.
- 25 Zheng, B., Zhang, Q., Zhang, Y., He, K. B., Wang, K., Zheng, G. J., Duan, F. K., Ma, Y. L., and Kimoto, T.: Heterogeneous chemistry: a mechanism missing in current models to explain secondary inorganic aerosol formation during the January 2013 haze episode in North China, *Atmos. Chem. Phys.*, 15, 2031–2049, <https://doi.org/10.5194/acp-15-2031-2015>, 2015.
- Zhu, J., Liao, H., Mao, Y., Yang, Y., and Jiang, H.: Interannual variation, decadal trend, and future change in ozone outflow from East Asia, *Atmospheric Chemistry and Physics*, 17, 3729-3747, 10.5194/acp-17-3729-2017, 2017.
- 30



Table 1. Model index, model version, parameterization schemes and reference for each participating model

Model Index	Model Version	Gas chemistry	Aerosol chemistry	Dry deposition	Wet scavenging	Meteorology	Boundary Condition	Online/Offline	References
M1	WRFCMAQ5.0.2	SAPRC99	Aero6 ISORROPIA(v2)	Wesely	Henry's law	Standard ^a	GEOS-Chem	Online access	Fu et al., (2008)
M2	WRFCMAQ5.0.2	SAPRC99	Aero6 ISORROPIA(v2)	Wesely	Henry's law	Standard ^a	Default	Online access	Wang et al., (2014b)
M3	WRFCMAQ5.0.1	CB05	Aero6 ISORROPIA(v2)	Wesely	Henry's law	Standard ^a	GEOS-Chem	Online access	Lam et al., (2011)
M4	WRFCMAQ4.7.1	SAPRC99	Aero5 ISORROPIA(v1.7)	Wesely	Henry's law	Standard ^a	CHASER	Offline	Itahashi et al., (2014)
M5	WRFCMAQ4.7.1	SAPRC99	Aero5 ISORROPIA(v1.7)	M3DRY	Henry's law	Standard ^a	CHASER	Offline	Yanagi et al., (2008)
M6	WRFCMAQ4.7.1	SAPRC99	Aero5 ISORROPIA(v1.7)	M3DRY	Henry's law	Standard ^a	CHASER	Offline	Nagashima et al., (2017)
M7	WRFCMAQ3.7.1	RACM	MADE/SORGAM	Wesely	Walcek and Taylor	Standard ^a	Default	Online integrated	Lee et al., (2017)
M8	WRFCMAQ3.6.1	RACM	MADE/VBS	Wesely	Henry's law	Standard ^a	CHASER	Online integrated	Lin et al., (2014)
M9	WRFCMAQ3.6	RADM2	MADE/SORGAM	Wesely	Easter	Standard ^a	GEOS-Chem	Online integrated	Chen et al., (2017)
M10	WRFCMAQ3.5.1	RADM2	GOCART	Wesely	Henry's law	WRF/MERRA2	MOZART/GOCART ^b	Online integrated	—
M11	NAQPMS	CBMZ	Aero5 ISORROPIA(v1.7)	Wesely	Henry's law	Standard ^a	CHASER	Online access	Wang et al., (2008)
M12	NHMChem	SAPRC99	ISORROPIA(v2)/MADM _S	Kajino, Zhang	Kajino, Pleim and Chang	JMA NHM	CHASER	Offline	Kajino et al., (2012)
M13	GEOS-Chem9.1.3	Bey	Park, Pye	Wesely	Liu	Geos-5	GEOS-Chem	Offline	Zhu et al., (2017)
M14	RAMSCMAQ4.6	SAPRC99	Aero5 ISORROPIA(v1.7)	Wesely	Henry's law	RAMS/NCEP	GEOS-Chem	Offline	Zhang et al., (2002)

^aStandard^a represents the reference meteorological field provided by MICS-Asia III project.

^bBoundary conditions used in M10 are taken from MOZART and GOCART (Chin et al., 2002; Horowitz et al., 2003), which provides results for gaseous pollutants and aerosols, respectively.

SAPRC99: Carter (2000). CB05: Yarwood (2005). Bey: Bey et al., (2001). CBMZ: Zaveri and Peters (1999). RACM: Stockwell et al., (1997). RADM2: Stockwell et al., (1990). Aero5 ISORROPIA (v1.7): Nenes et al., (1998). Aero6 ISORROPIA (v2): Fountoukis and Nenes (2007). Park: Park et al., (2004). Pye: Pye et al., (2009). MADE-VBS: Tuccella et al., (2015). MADE: Ackermann et al., (1998). M3DRY: Pleim et al., (2001). Wesely: Wesely (1989). Kajino: Kajino et al., (2012). Zhang: Zhang et al., (2001). Liu: Liu et al., (2001). Pleim and Chang: Pleim and Chang (1992). Easter: Easter et al., (2004). Walcek and Taylor: Walcek and Taylor (1986).

**Table 2. Aerosol species simulated by each participating model**

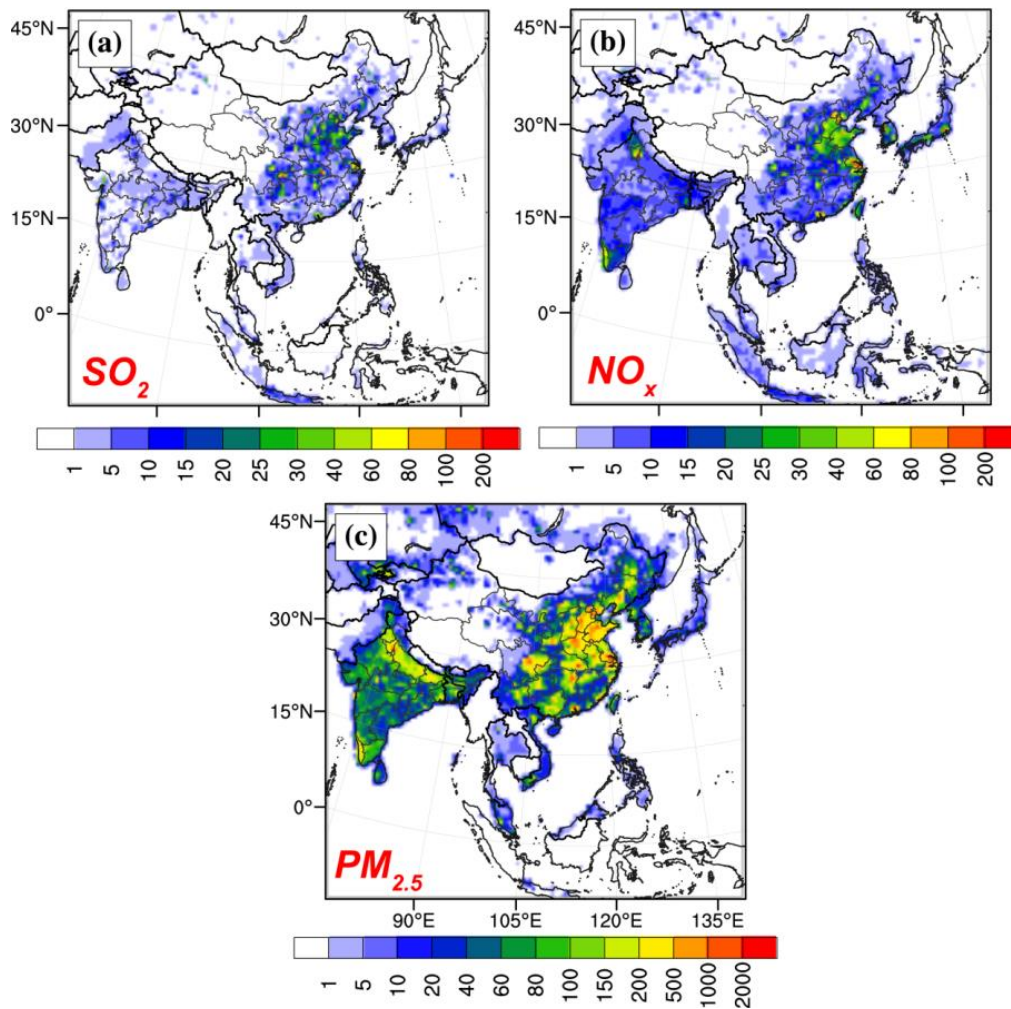
Model Index	BC	OC	SO ₄ ²⁻	NO ₃ ⁻	NH ₄ ⁺	PM _{2.5}	PM ₁₀	AOD
M1	Y	Y	Y	Y	Y	Y	Y	Y
M2	Y	Y	Y	Y	Y	Y	Y	Y
M3	Y	Y	Y	Y	Y	Y	Y	Y
M4	Y	Y	Y	Y	Y	Y	Y	Y
M5	Y	Y	Y	Y	Y	Y	Y	—
M6	Y	Y	Y	Y	Y	Y	Y	—
M7	Y	—	Y	Y	Y	Y	Y	Y
M8	Y	Y	Y	Y	Y	Y	Y	—
M9	—	—	Y	Y	Y	Y	Y	Y
M10	—	—	—	—	—	—	—	—
M11	Y	Y	Y	Y	Y	Y	Y	Y
M12	Y	Y	Y	Y	Y	Y	Y	Y
M13	Y	Y	Y	Y	Y	Y	—	Y
M14	Y	Y	Y	Y	Y	Y	Y	Y

“Y” means aerosol species is analyzed in this manuscript.



Table 3. Performance statistics of BC, SO_4^{2-} , NO_3^- , NH_4^+ , $\text{PM}_{2.5}$, PM_{10} and AOD. Best results are set to be bold with underline. The mean observation of each species and the number of observations are also given with italic. In this table, observed monthly mean values from EANET, CNEMC and AERONET are used (except BC, the monthly BC concentrations are collected from published documents).

Species	Statistics	M1	M2	M4	M5	M6	M7	M8	M9	M11	M12	M13	M14	EM
BC (5.0 $\mu\text{g m}^{-3}$) (<i>nstd=5</i>)	R	0.70	0.73	0.71	0.65	0.70	0.73	0.80	–	0.69	0.68	0.75	0.72	0.73
	NMB(%)	1.0	12.7	-24.7	-54.9	-17.8	-11.7	-34.2	–	-17.5	-2.2	-26.8	-11.6	-17.0
	RMSE	4.10	4.30	2.95	4.06	2.99	2.69	2.84	–	2.91	3.52	2.80	2.64	2.77
SO_4^{2-} (3.8 $\mu\text{g m}^{-3}$) (<i>nstd=31</i>)	R	0.69	0.71	0.64	0.58	0.66	0.48	0.53	0.65	0.55	0.50	0.76	0.46	0.69
	NMB(%)	-23.1	-13.0	-31.0	-26.4	-26.9	-67.7	-1.6	-67.0	-34.5	23.2	-31.9	69.3	-19.1
	RMSE	3.21	3.00	3.46	3.57	3.35	4.64	3.62	4.45	3.78	4.01	3.24	5.51	3.22
NO_3^- (1.7 $\mu\text{g m}^{-3}$) (<i>nstd=31</i>)	R	0.55	0.51	0.62	0.65	0.58	0.45	0.29	0.64	0.59	0.60	0.43	0.58	0.65
	NMB(%)	9.0	-7.2	-42.7	-1.7	-11.8	-81.2	-80.6	125.7	46.5	54.0	22.7	35.4	4.9
	RMSE	2.70	2.71	2.48	2.29	2.46	3.37	3.18	4.37	2.89	2.80	2.96	2.62	2.27
NH_4^+ (1.1 $\mu\text{g m}^{-3}$) (<i>nstd=31</i>)	R	0.67	0.64	0.68	0.66	0.69	0.55	0.34	0.75	0.66	0.62	0.64	0.68	0.71
	NMB(%)	23.2	33.7	-10.6	7.4	14.6	-93.5	-34.2	45.3	35.0	49.9	34.9	56.3	14.0
	RMSE	1.24	1.42	1.15	1.21	1.16	1.83	1.53	1.26	1.27	1.54	1.29	1.47	1.11
$\text{PM}_{2.5}$ (51.4 $\mu\text{g m}^{-3}$) (<i>nstd=14</i>)	R	0.80	0.78	0.80	0.71	0.80	0.80	0.77	0.82	0.80	0.78	0.75	0.81	0.83
	NMB(%)	10.0	13.6	-1.3	-25.3	-5.8	-5.7	-15.3	26.2	5.2	31.4	-26.5	46.0	4.4
	RMSE	27.56	34.88	23.03	28.00	21.80	23.54	24.83	28.52	22.06	34.87	27.10	35.85	21.23
PM_{10} (80.7 $\mu\text{g m}^{-3}$) (<i>nstd=51</i>)	R	0.75	0.74	0.74	0.65	0.75	0.70	0.70	0.66	0.78	0.82	–	0.63	0.78
	NMB(%)	-40.7	-38.7	-35.7	-55.7	-46.6	-43.7	-43.4	-16.9	-25.4	-18.8	–	7.1	-32.6
	RMSE	51.31	50.88	49.10	64.55	55.31	55.07	55.11	50.67	42.91	37.28	–	47.26	45.81
AOD (0.2) (<i>nstd=38</i>)	R	0.64	0.55	0.56	–	–	0.54	–	0.60	0.69	0.66	0.71	0.57	0.68
	NMB(%)	-2.0	63.7	-28.5	–	–	-21.8	–	11.1	73.1	-6.2	47.1	36.7	18.7
	RMSE	0.15	0.22	0.16	–	–	0.18	–	0.19	0.22	0.13	0.25	0.22	0.14



5 **Figure 1:** The merged emission inventories of MIX emission, MEGAN biogenic emission, GFED biomass burning emission, air and ship emission, and volcanic emission for SO_2 , NO_x and $\text{PM}_{2.5}$ in 2010. The unit for gas is Mmol/month/grid , and the unit for aerosol is Mg/month/grid .

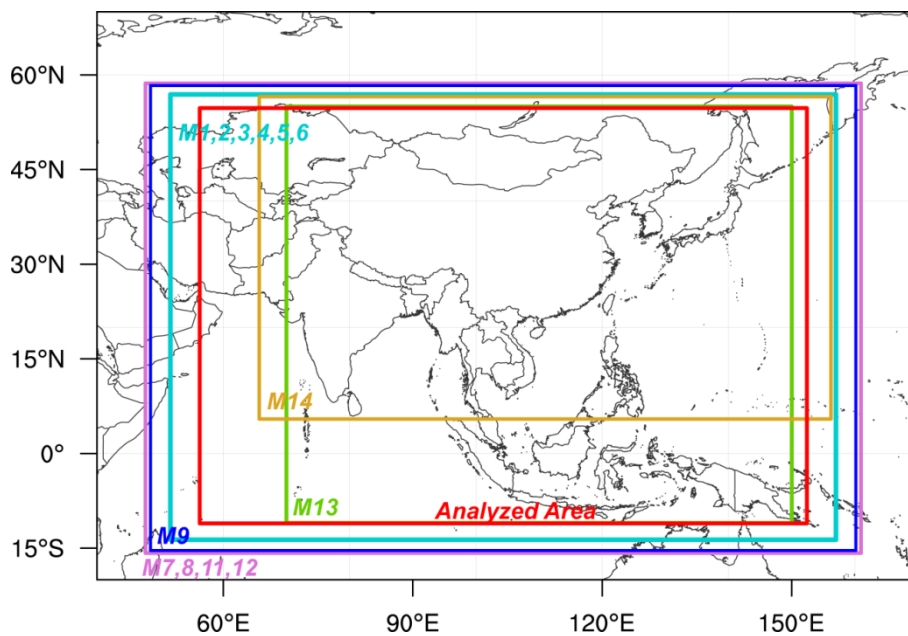


Figure 2: Simulation domain for each participating model and the final analyzed area used in this manuscript.

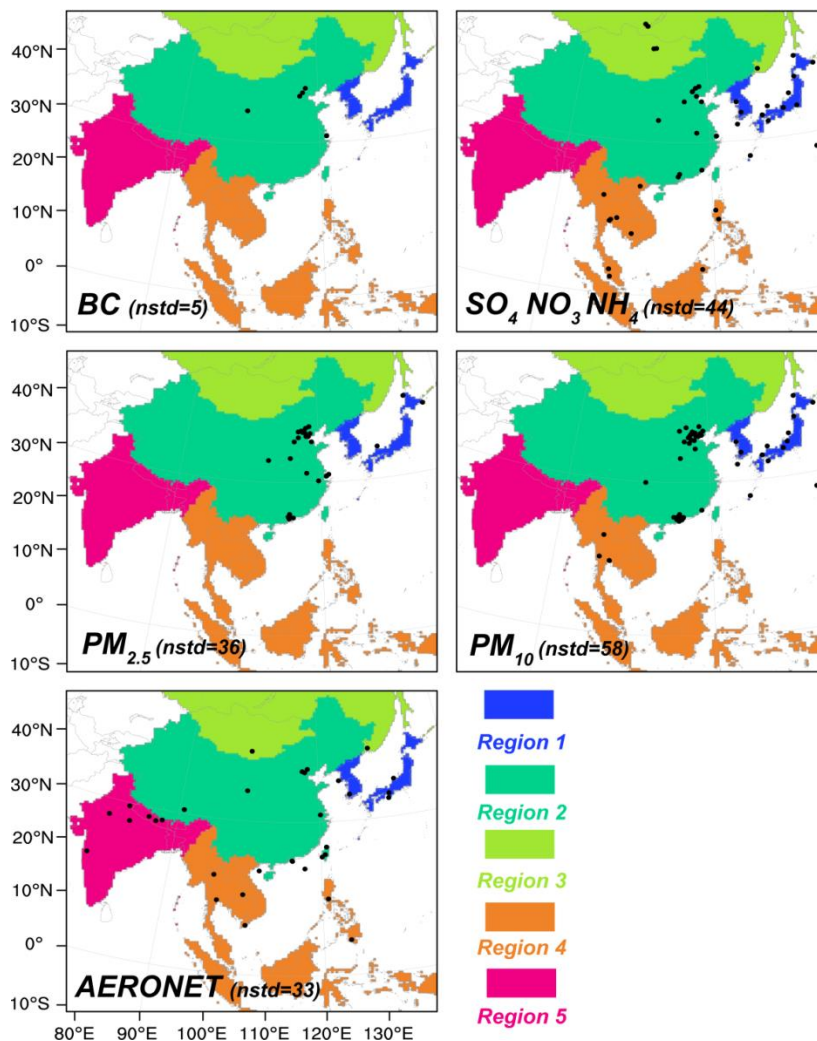
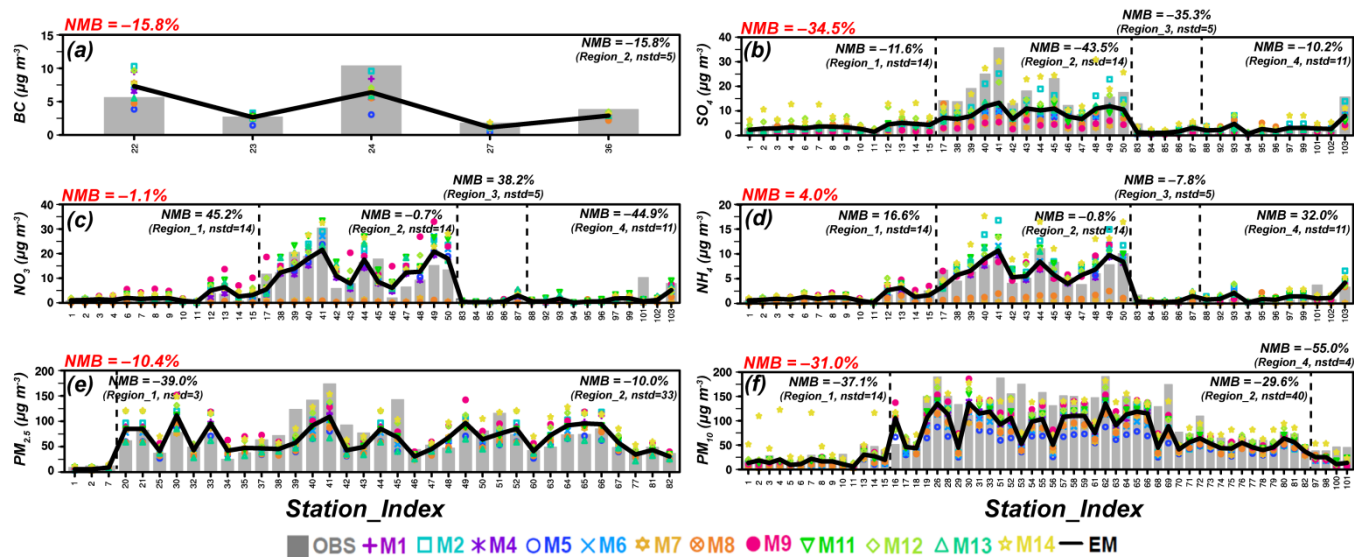
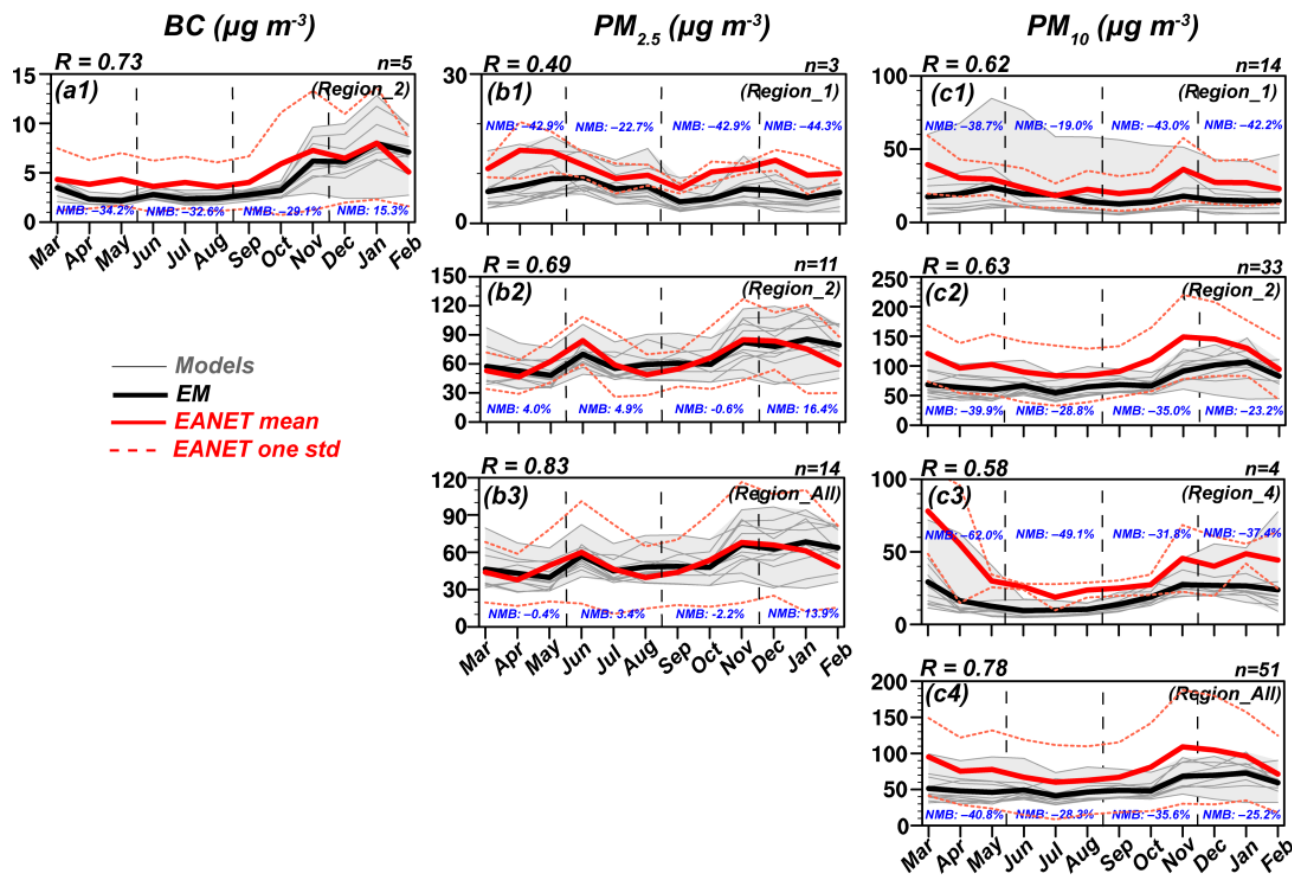


Figure 3: Spatial distribution of observation sites for each species. Five designed regions are also shown in each panel.



5 **Figure 4:** Comparison of observed and simulated concentrations of (a) BC, (b) SO_4^{2-} , (c) NO_3^- , (d) NH_4^+ , (e) $\text{PM}_{2.5}$ and (f) PM_{10} . In
 each panel, the gray bars show observation data, the colored dots represent simulation results from participating models, and the
 black solid line is the ensemble mean. The numbers on x-axis represent the monitoring sites, and the information of these sites is
 listed in Table S1. Normalized mean biases (NMBs) between observations and ensemble means in each defined region (with black
 color) and the entire analyzed area (with red color) are also shown. In this picture, observed annual mean values from EANET,
 10 CNEMC and published documents are used.



5
 10
 15
 Figure 5: Observed and simulated seasonal cycle of aerosol species. (a1) BC, (b1)-(b3) $PM_{2.5}$, (c1)-(c4) PM_{10} . Simulations and observations are grouped into five defined regions as illustrated in Figure 3, with each model sampled at the corresponding monitoring sites in each region before averaging together. Individual models are represented by the thin grey lines, with the grey shaded area indicating their spread. The thick black line is the ensemble mean. The red solid line is the observational mean and the dashed red lines mean one standard deviation for each group of stations. The correlations (R_s , with black color) and normalized mean biases (NMBs, with blue color) for ensemble means versus observations during each season (spring: from March to May; summer: from June to August; autumn: from September to November; winter: January, February and December) and the entire year are shown in each panel. Also shown is the number of monitoring sites participating in calculating statistics in each region. In this picture, observed monthly mean values from EANET and CNEMC are used (except BC, the monthly BC concentrations are collected from published documents).

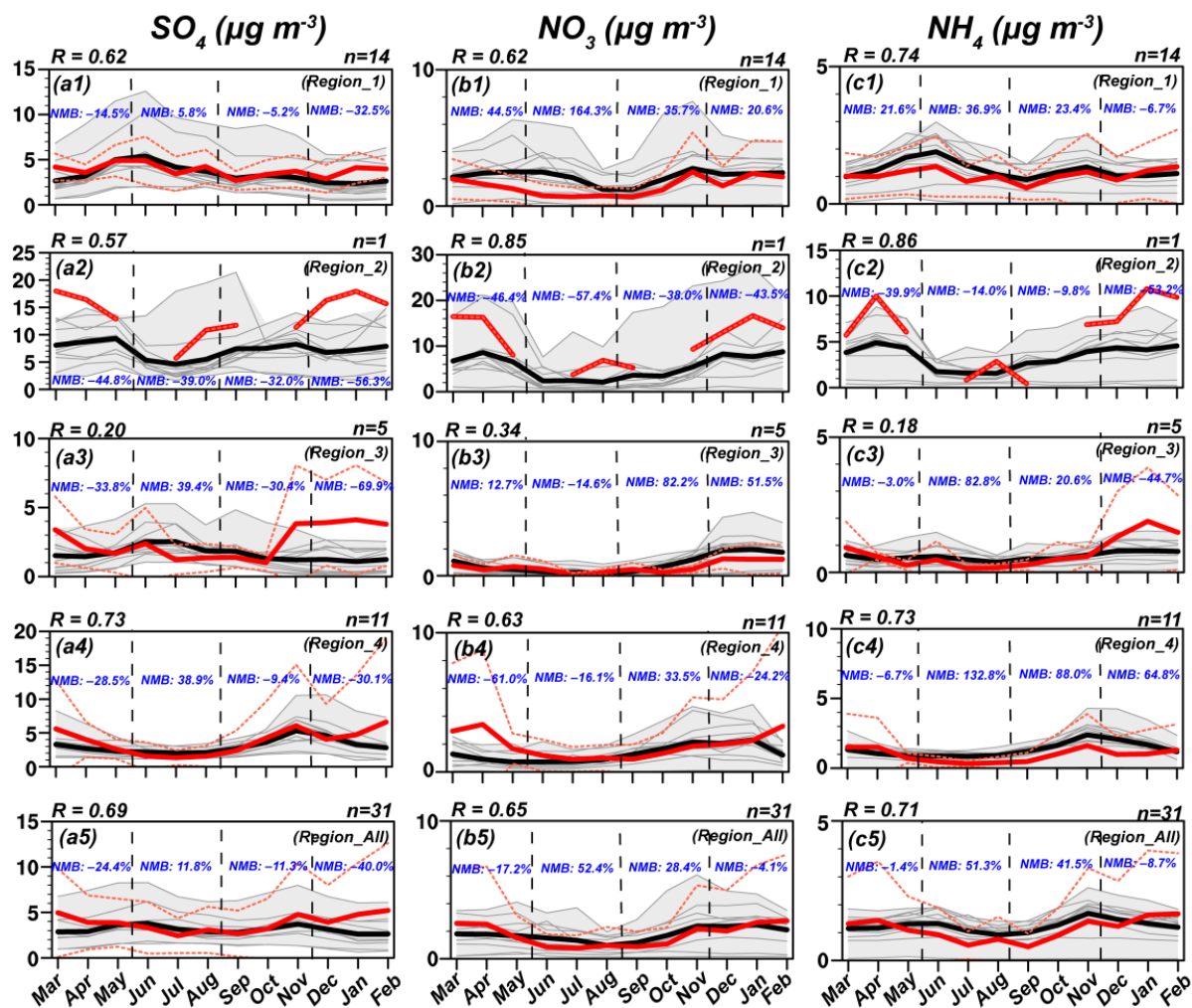
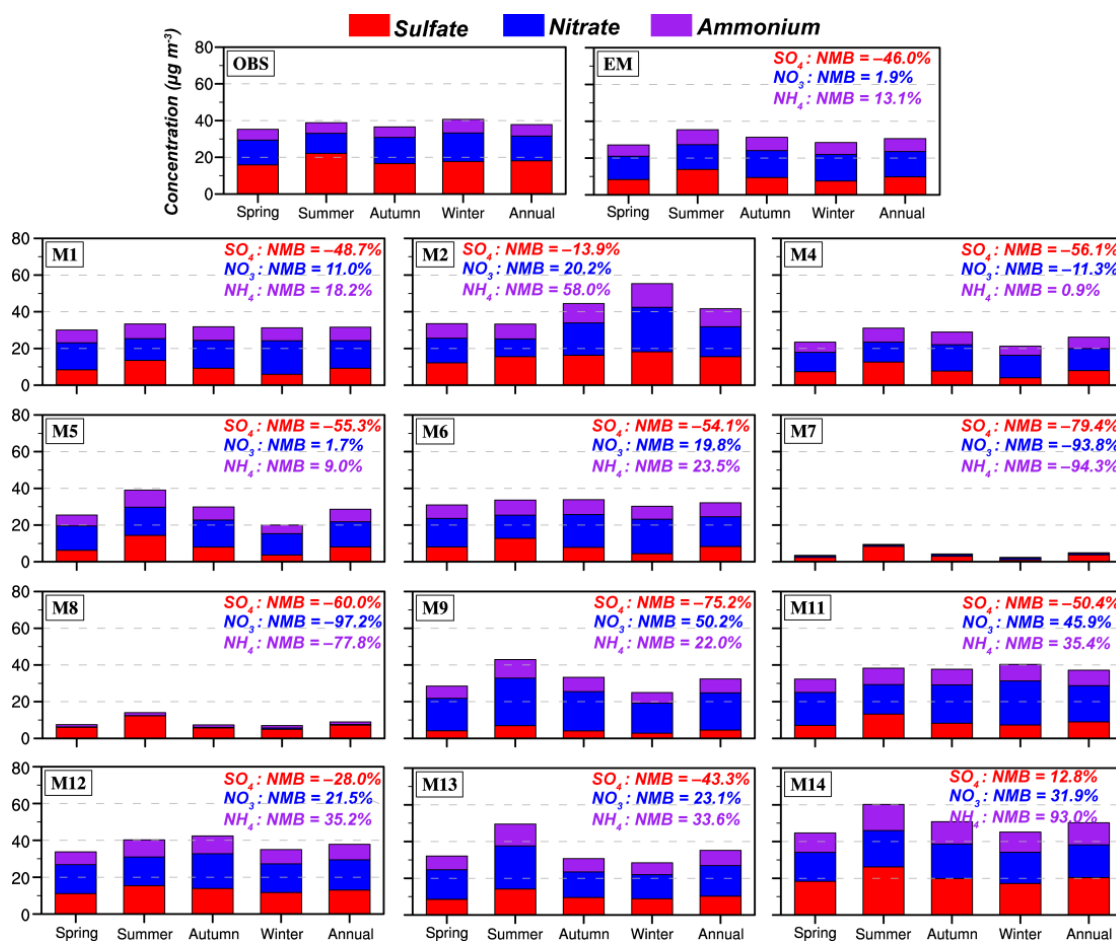
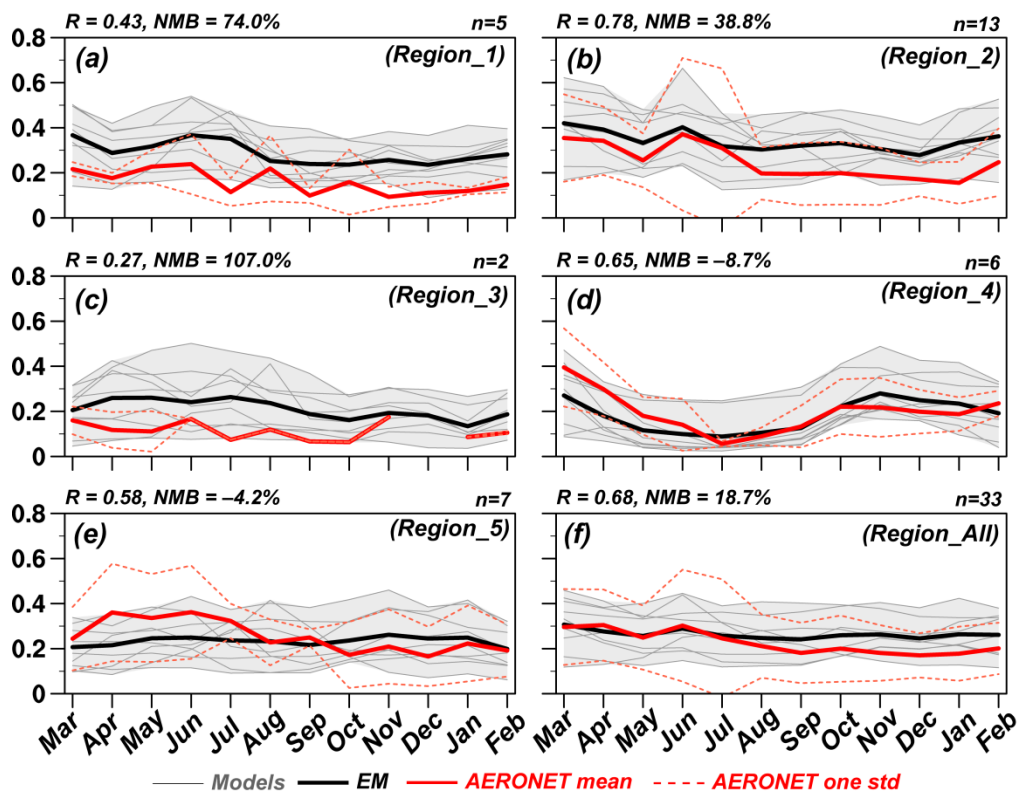


Figure 6: Same as Figure 5, but for SO_4^{2-} (a1-a5), NO_3^- (b1-b5) and NH_4^+ (c1-c5). In this picture, only monthly EANET observations are used.

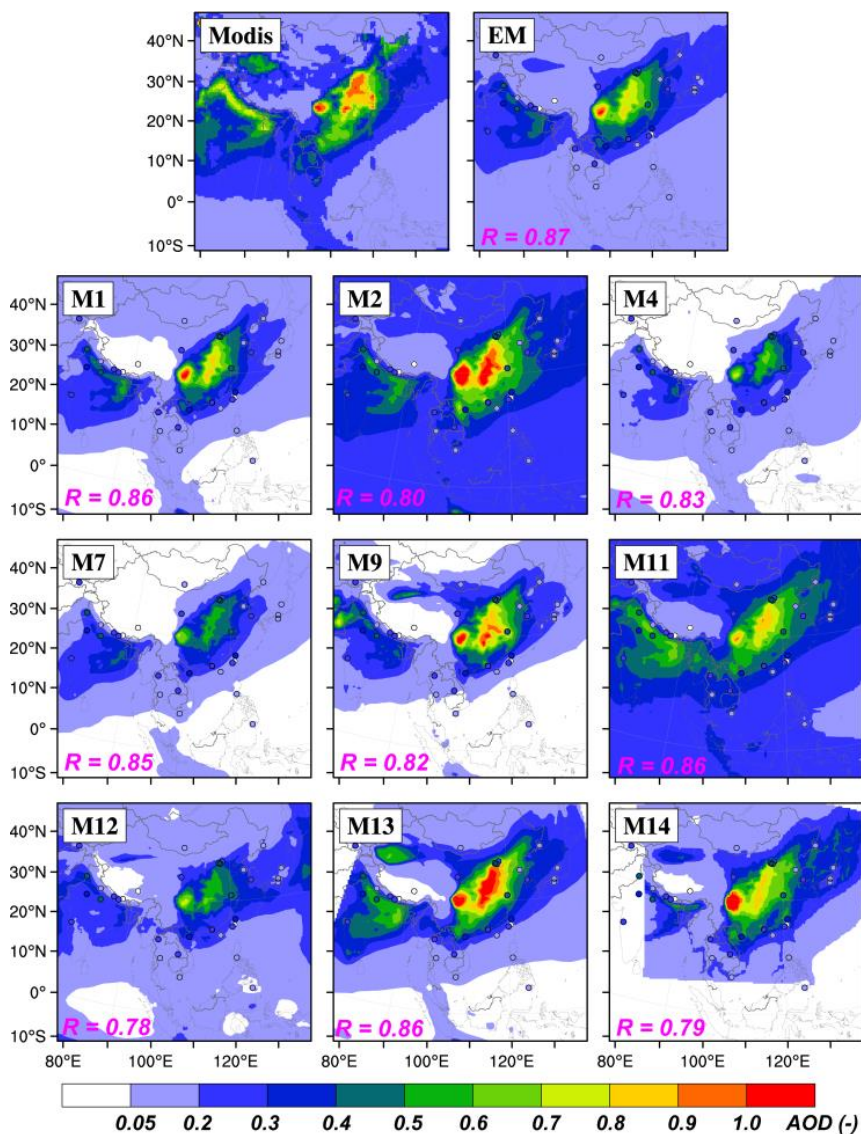
5



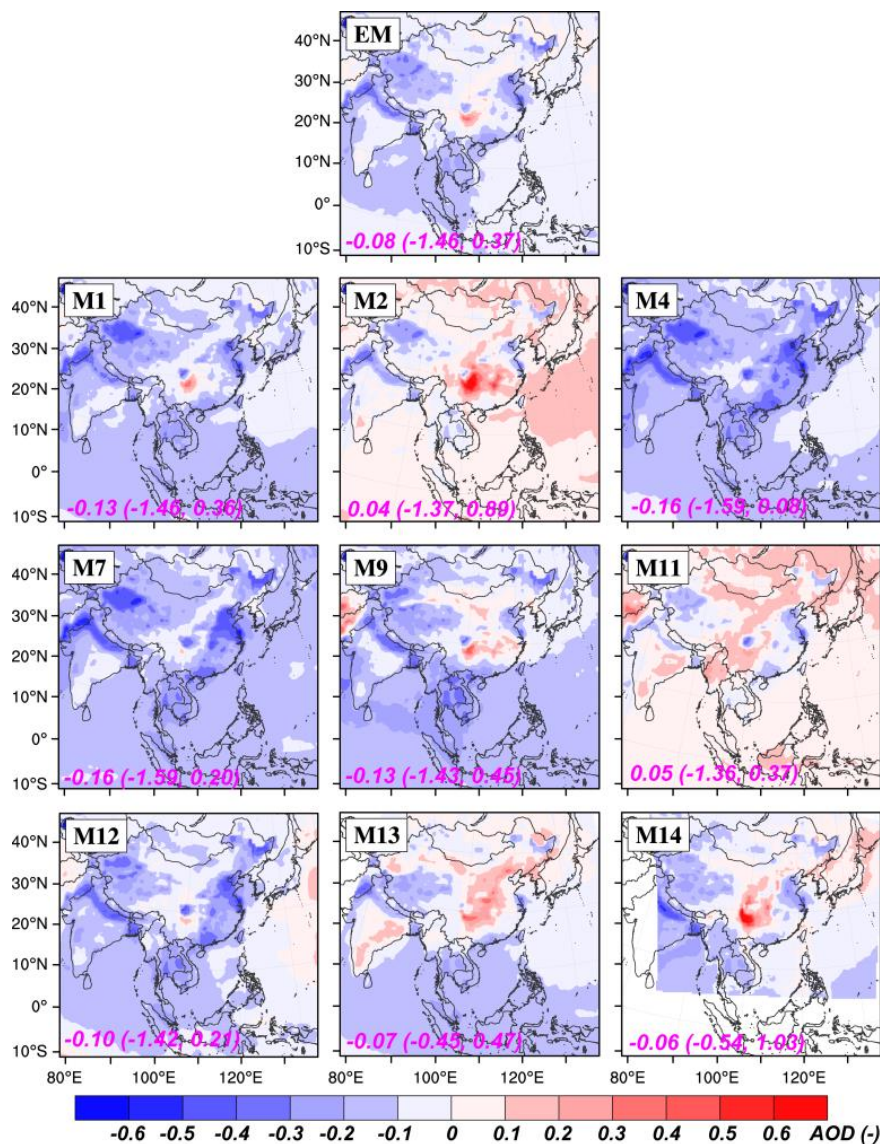
5 **Figure 7: Observed and simulated seasonal mean concentrations of SO_4^{2-} , NO_3^- and NH_4^+ in Region_2. Normalized mean biases (NMBs) of SO_4^{2-} (with red color), NO_3^- (with blue color) and NH_4^+ (with purple color) for each participating model and the ensemble model are also shown. In this picture, seasonal observations are collected from published documents.**



5 Figure 8: Similar as Figure 5, but for comparison of seasonal cycle of aerosol optical depth (AOD) at 550 nm between simulations and AERONET observations in each defined region. (a) Region_1, (b) Region_2, (c) Region_3, (d) Region_4, (e) Region_5, and (f) Region_All.



5 **Figure 9: Spatial distribution of aerosol optical depth (AOD) at 550 nm retrieved by MODIS and simulated by participating models. The spatial correlation coefficients are given in the bottom left corner of each panel. Observed AOD from AERONET stations are also shown.**



5 **Figure 10: Spatial distribution of the differences between MODIS AOD and simulation results. The domain mean difference (the minimum difference, the maximum difference) are also listed in the bottom left corner of each panel.**

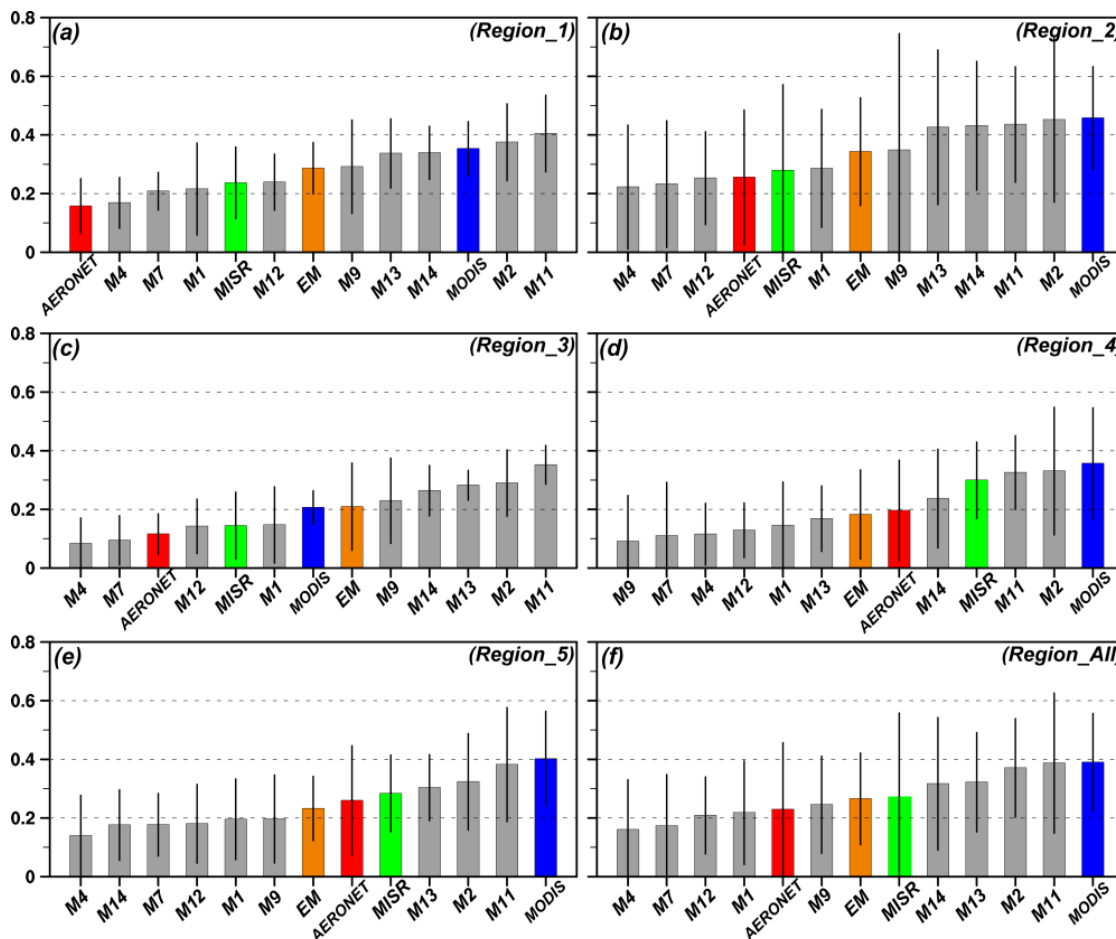


Figure 11: Multi-model AOD (grey bars) averaged over the five defined regions (Region_1 to Region_5) and the whole analyzed domain (Region_All), together with the ensemble mean predictions (orange bar), measured values retrieved from MODIS (blue bar) and MISR (green bar). AOD averaged over the corresponding AERONET stations (red bar) in each region are also shown. The error bars represent one standard deviation. (a) Region_1, (b) Region_2, (c) Region_3, (d) Region_4, (e) Region_5, and (f) Region_All.

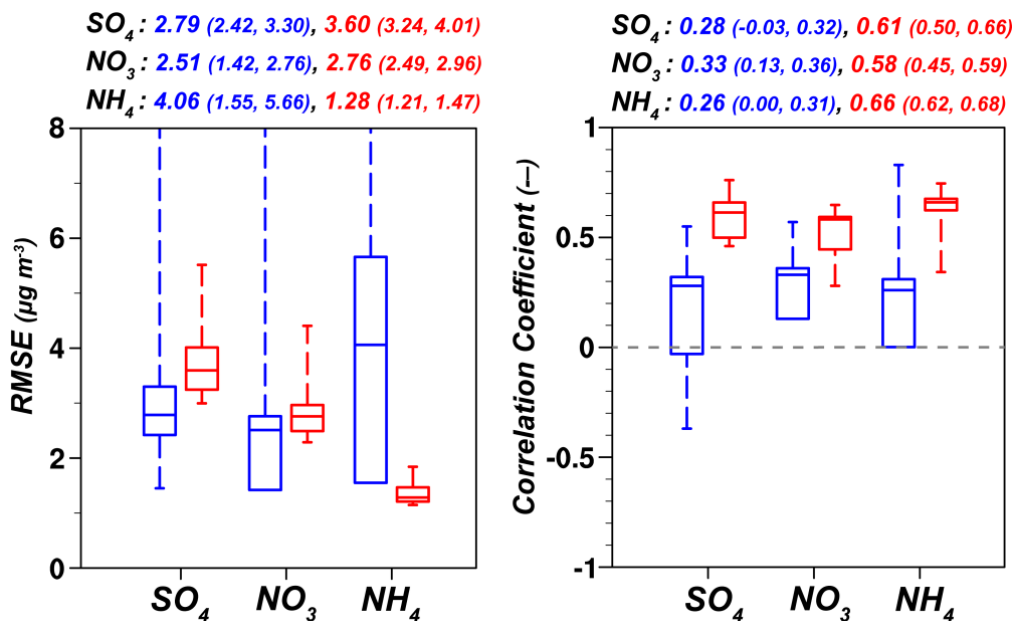
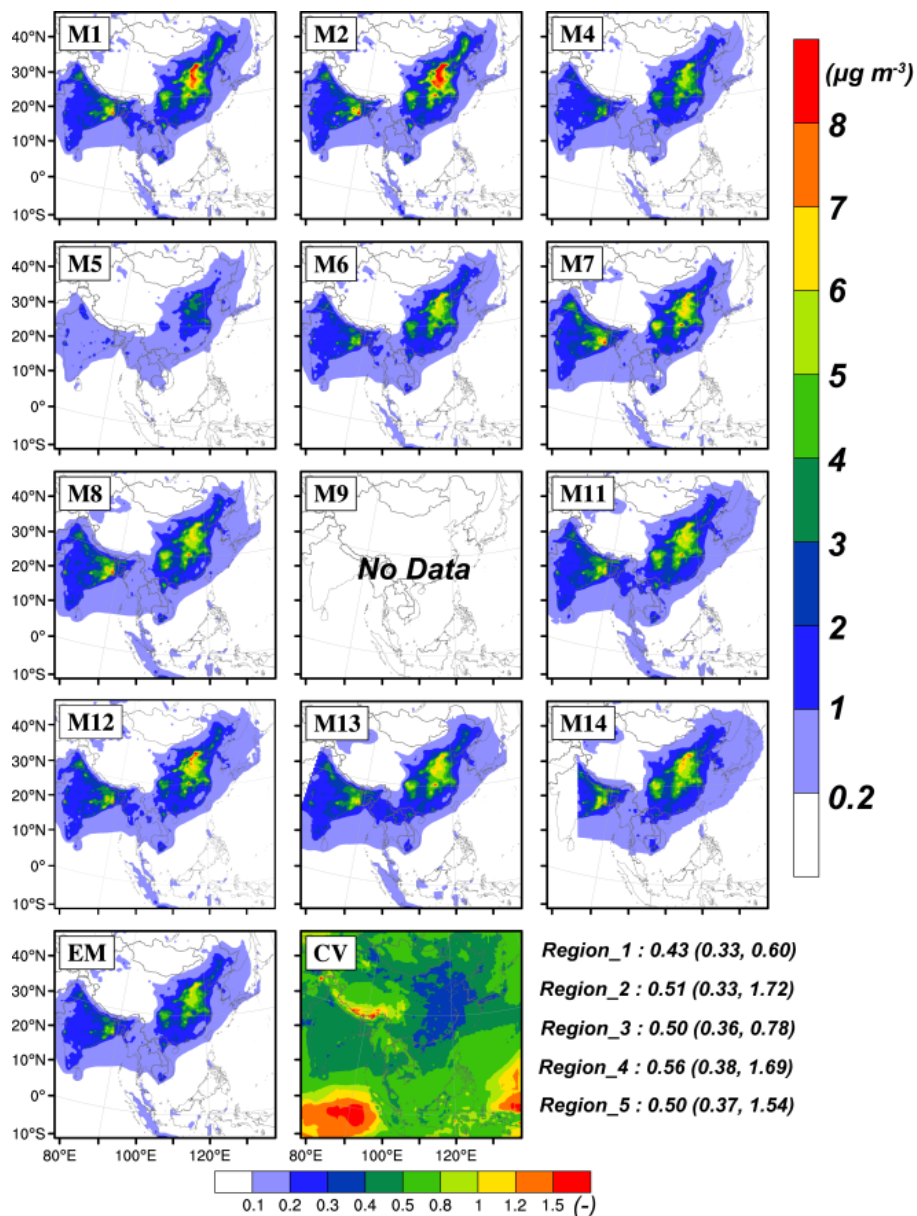


Figure 12: Intercomparison of model performance in MICS-Asia II (blue) and MICS-Asia III (red) for SO_4^{2-} , NO_3^- and NH_4^+ . Eight models participated in MICS-Asia Phase II. Detailed information can be found in Hayami et al. (2008). Twelve models are analyzed in MICS-Asia Phase III. Statistics (e.g. RMSE and R) are calculated from all the available models against monthly observations provided by EANET. Each boxplot summarizes the statistical information including the interquartile range, the full range and the median. Detailed values of medians (interquartile ranges) for SO_4^{2-} , NO_3^- and NH_4^+ are also listed at the top of each panel.



5 **Figure 13: Spatial distribution of simulated BC concentrations from each participating model and the multi-model ensemble mean. The coefficient of variation (CV), defining as the standard deviation of these models divided by their mean, is also calculated. The values listed in the bottom right corner represent the averaged CV (the minimum CV, the maximum CV) in each defined region.**

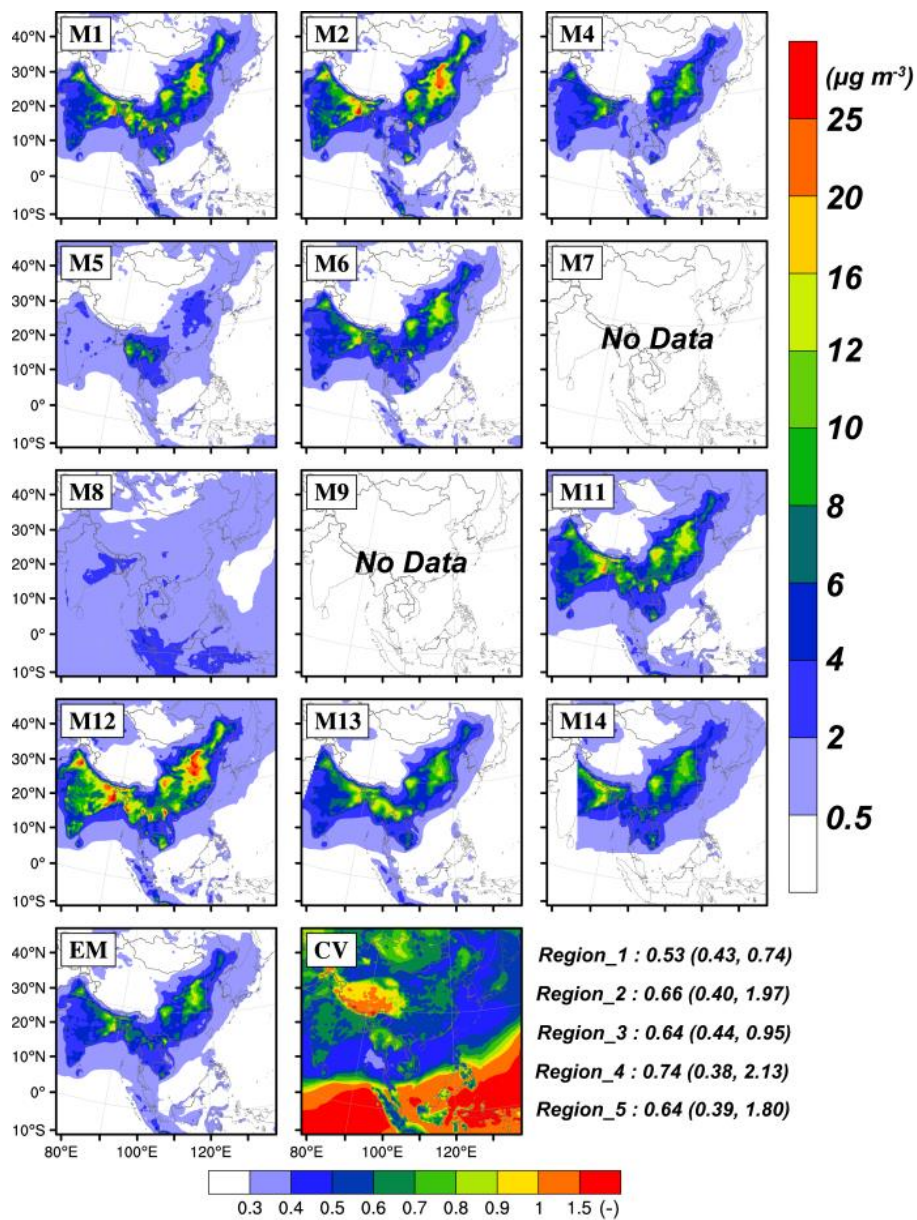


Figure 14: Similar as Figure 13, but for OC.

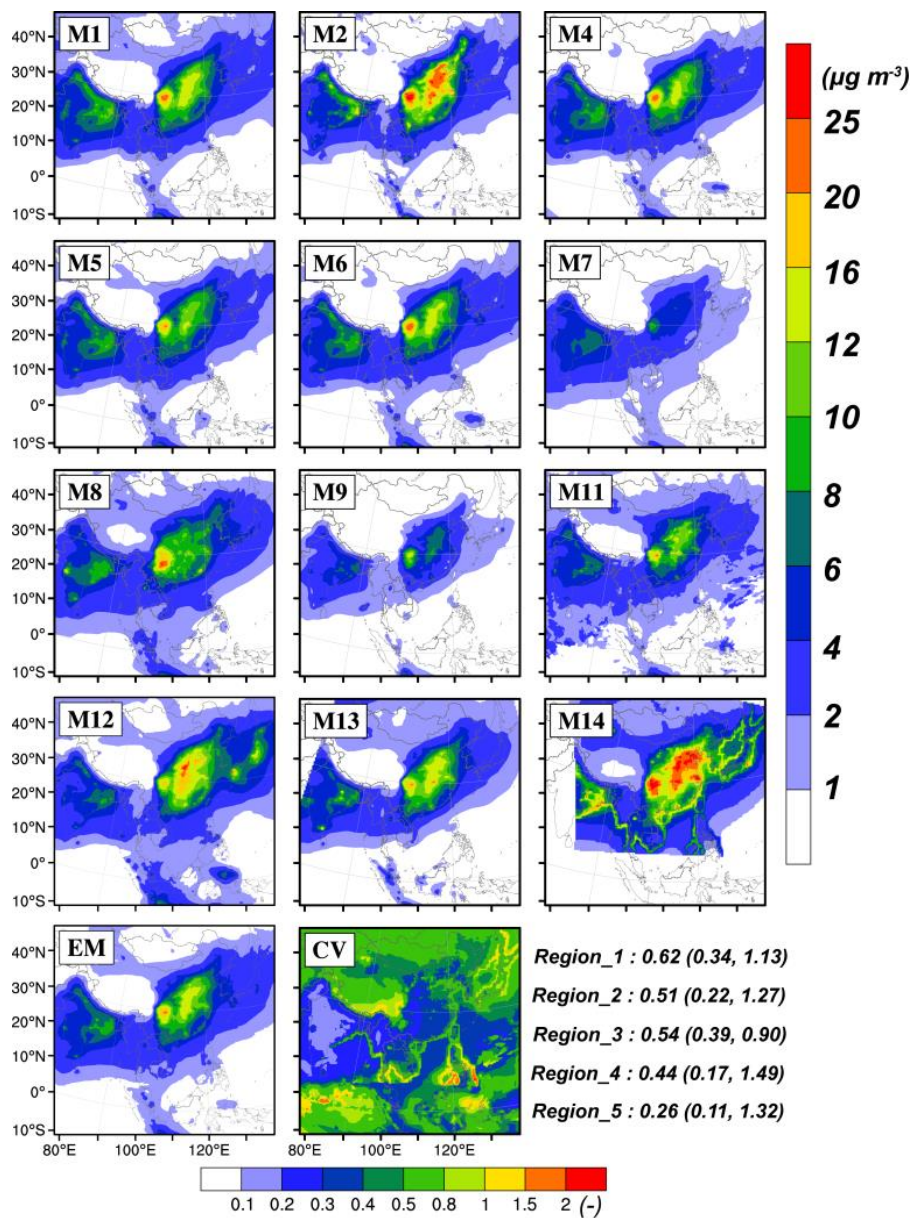


Figure 15: Similar as Figure 13, but for SO_4^{2-} .

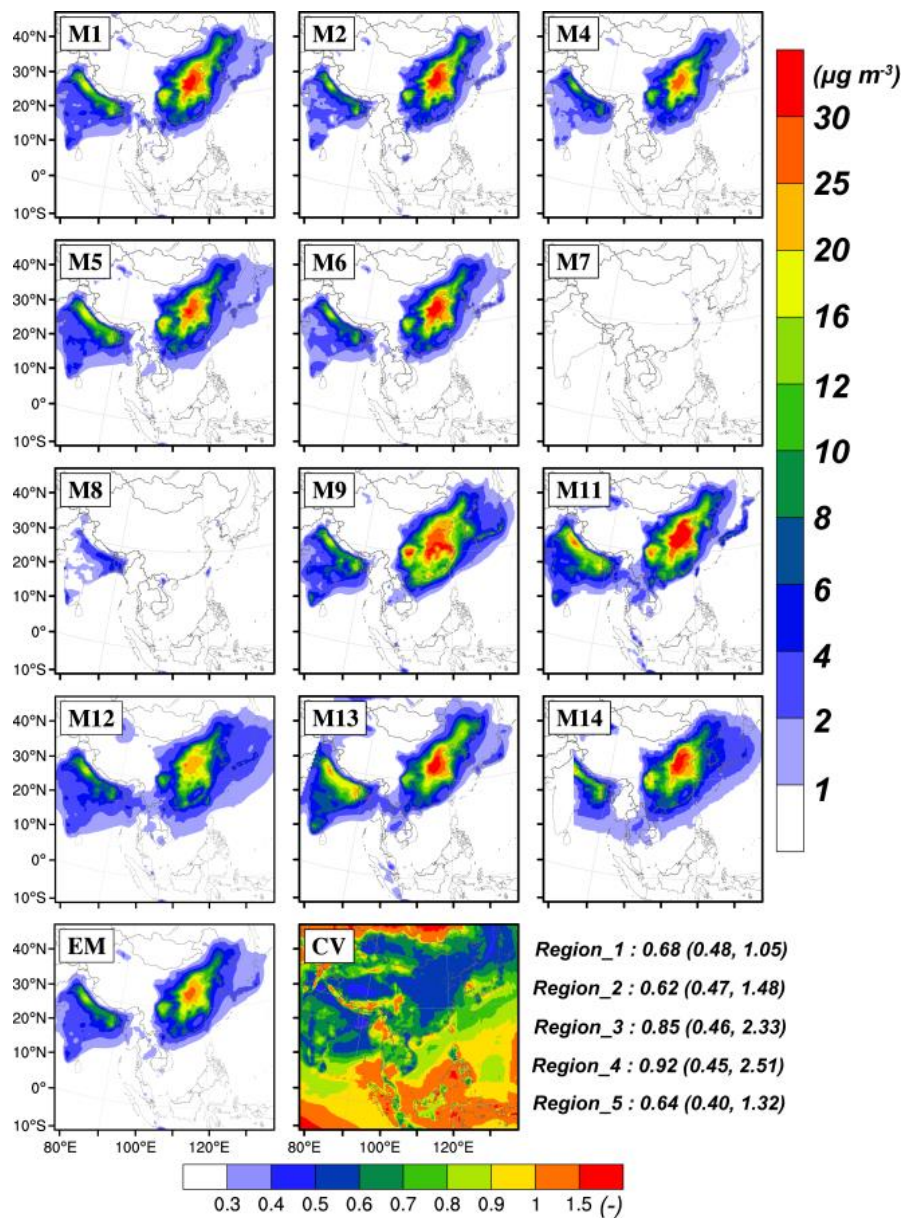


Figure 16: Similar as Figure 13, but for NO_3^- .

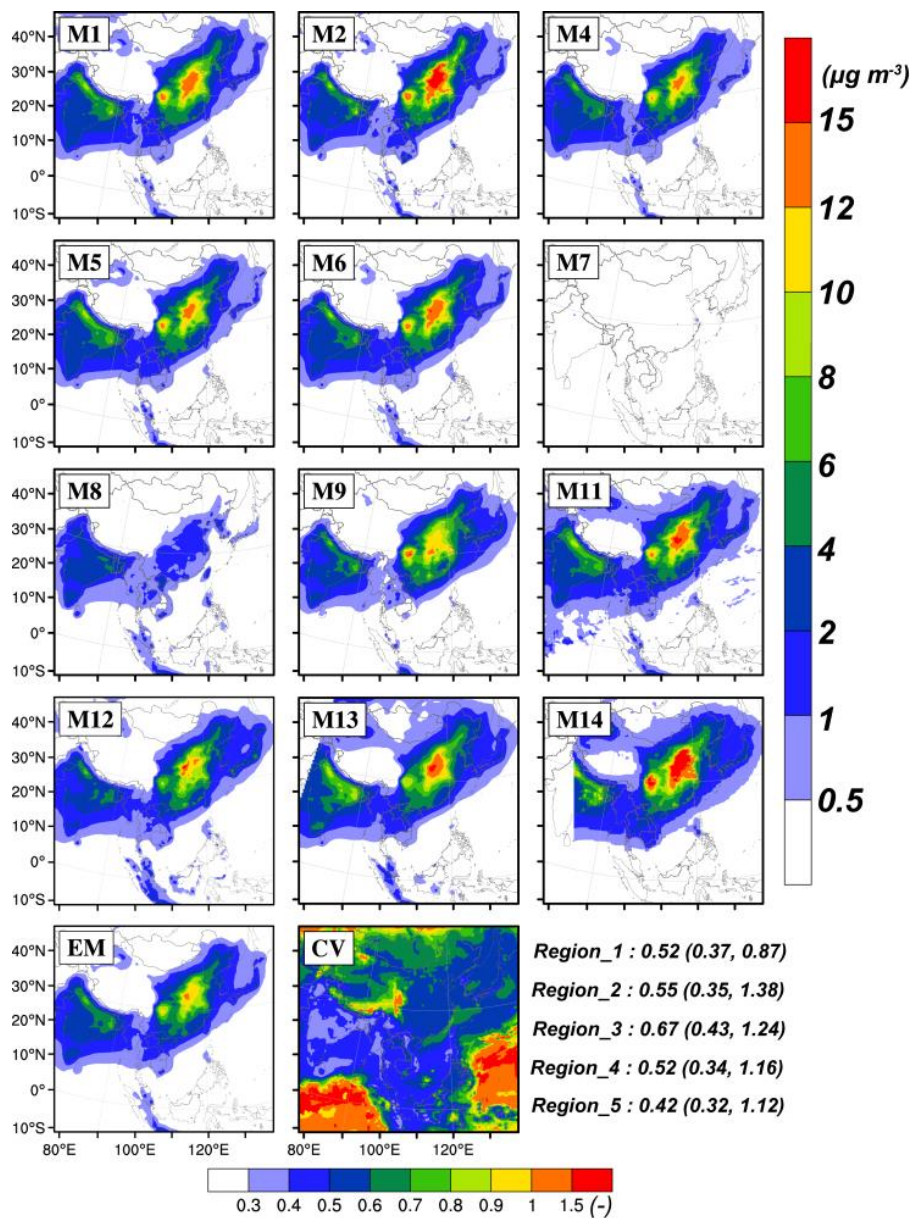


Figure 17: Similar as Figure 13, but for NH_4^+ .

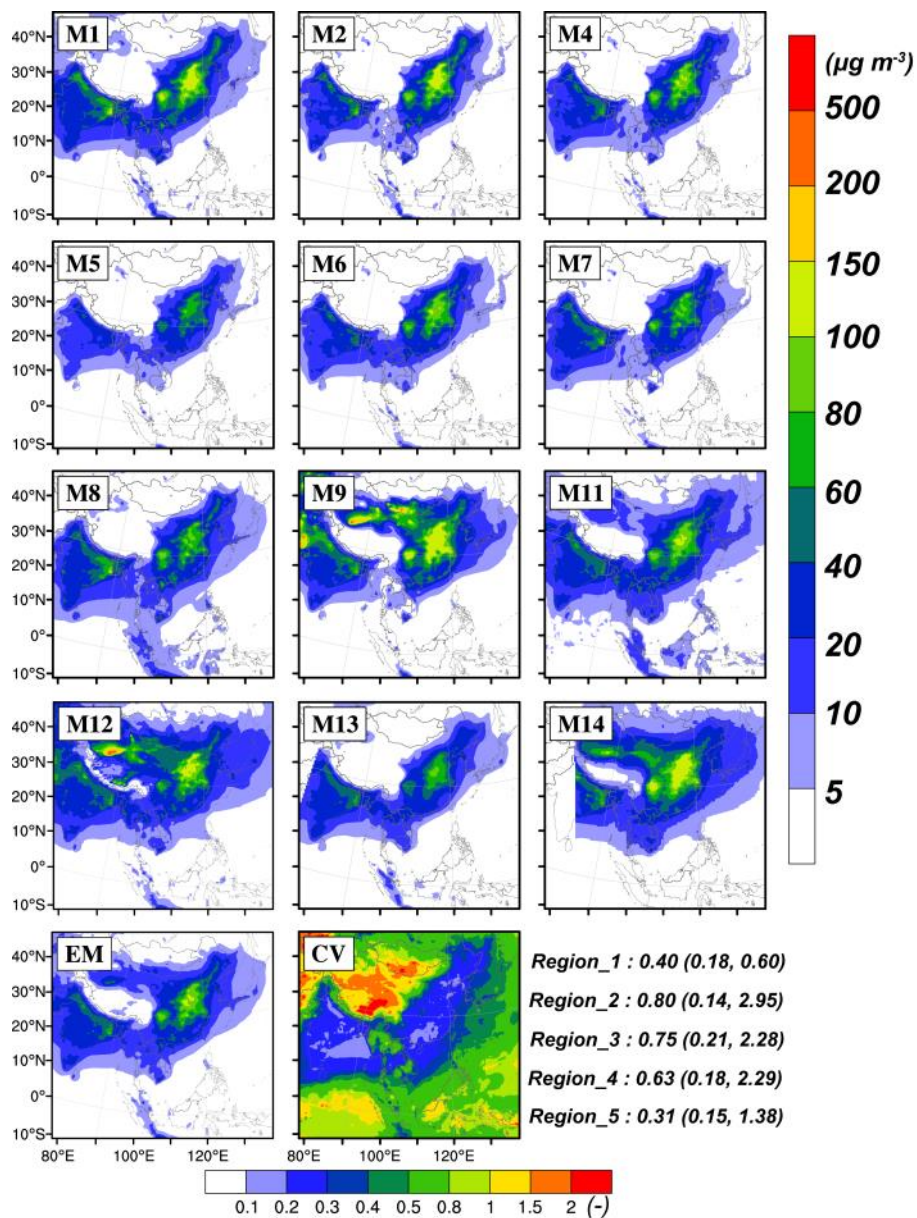


Figure 18: Similar as Figure 13, but for $\text{PM}_{2.5}$.

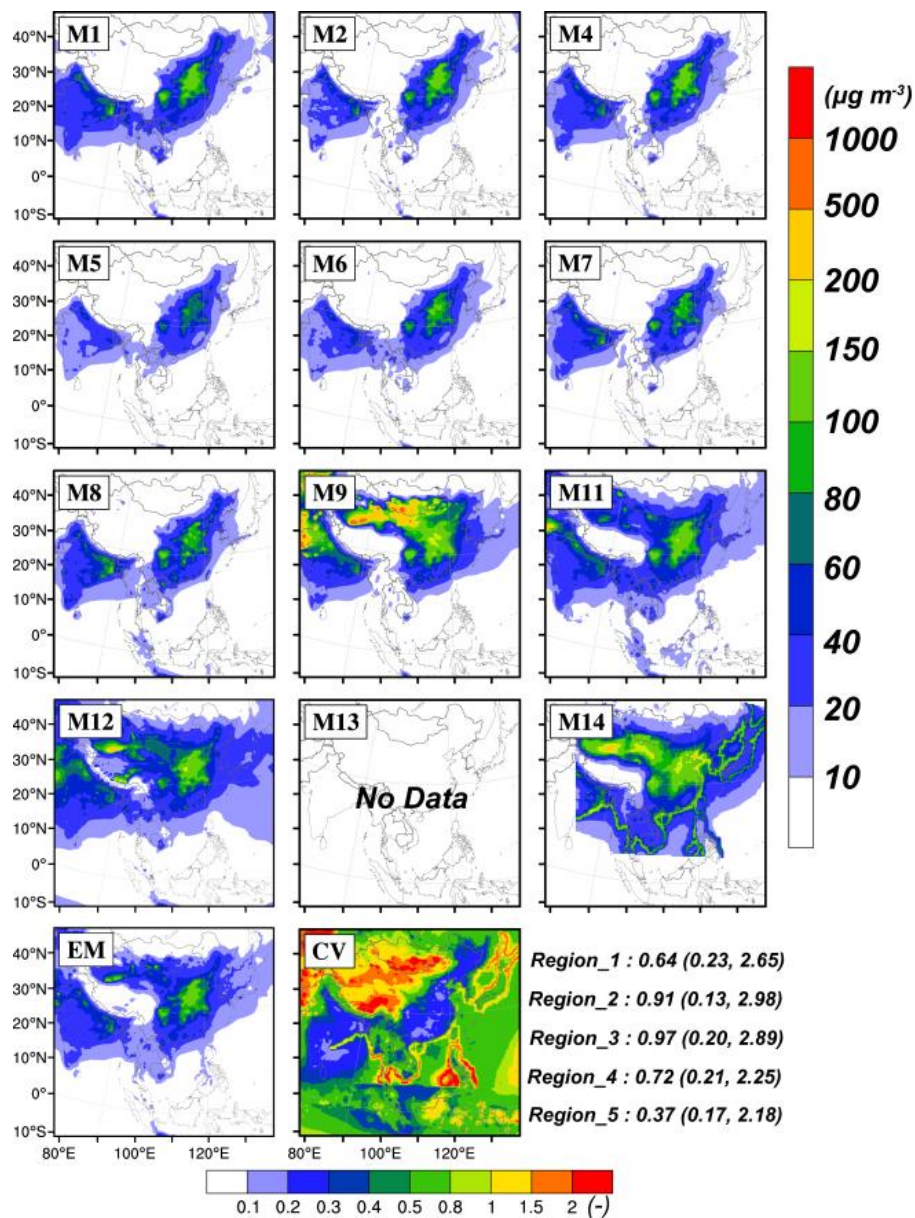


Figure 19: Similar as Figure 13, but for PM₁₀.

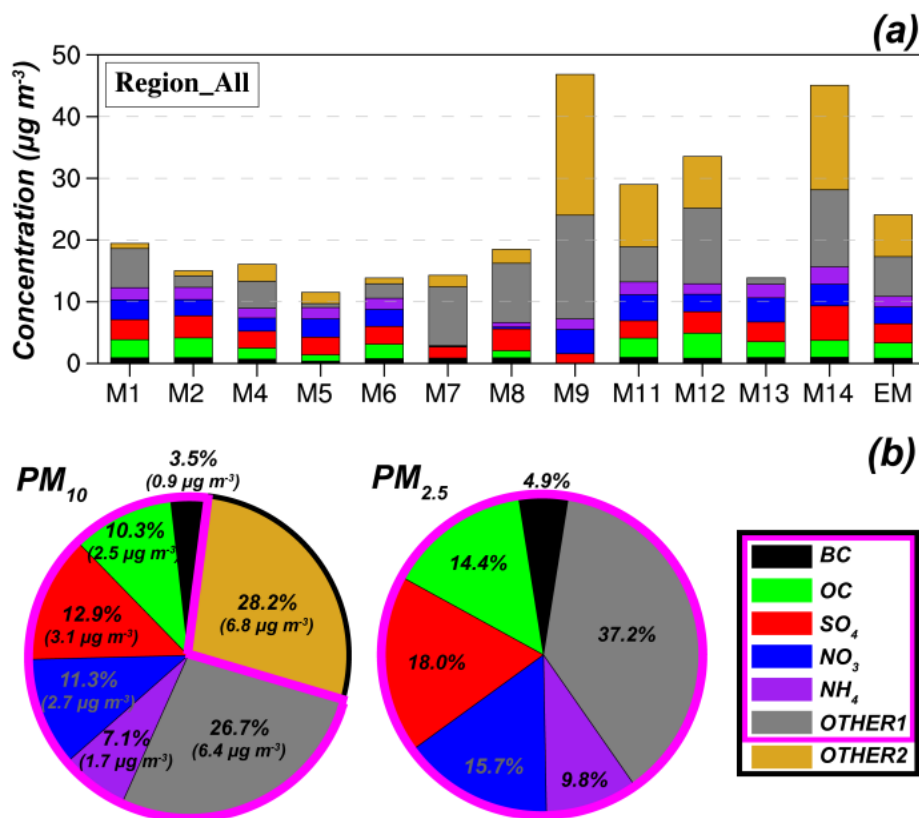
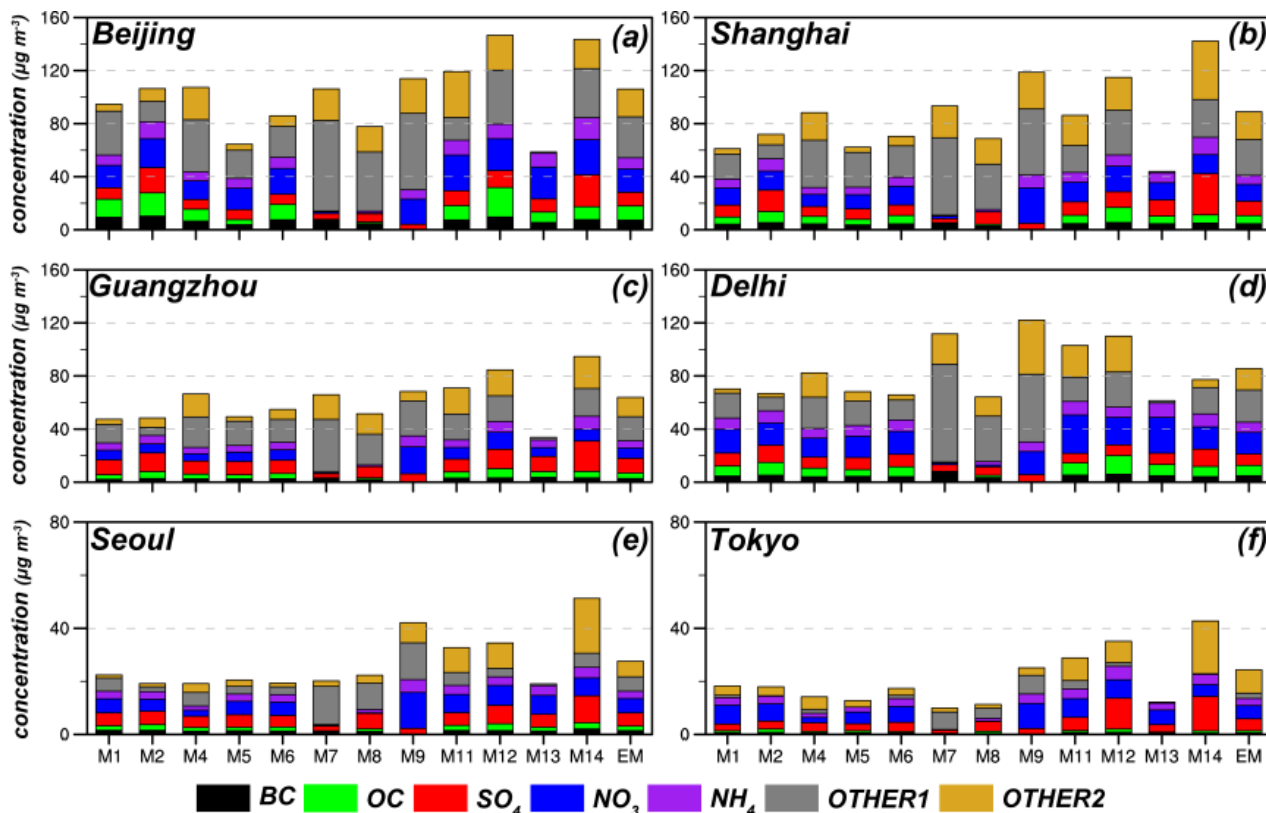
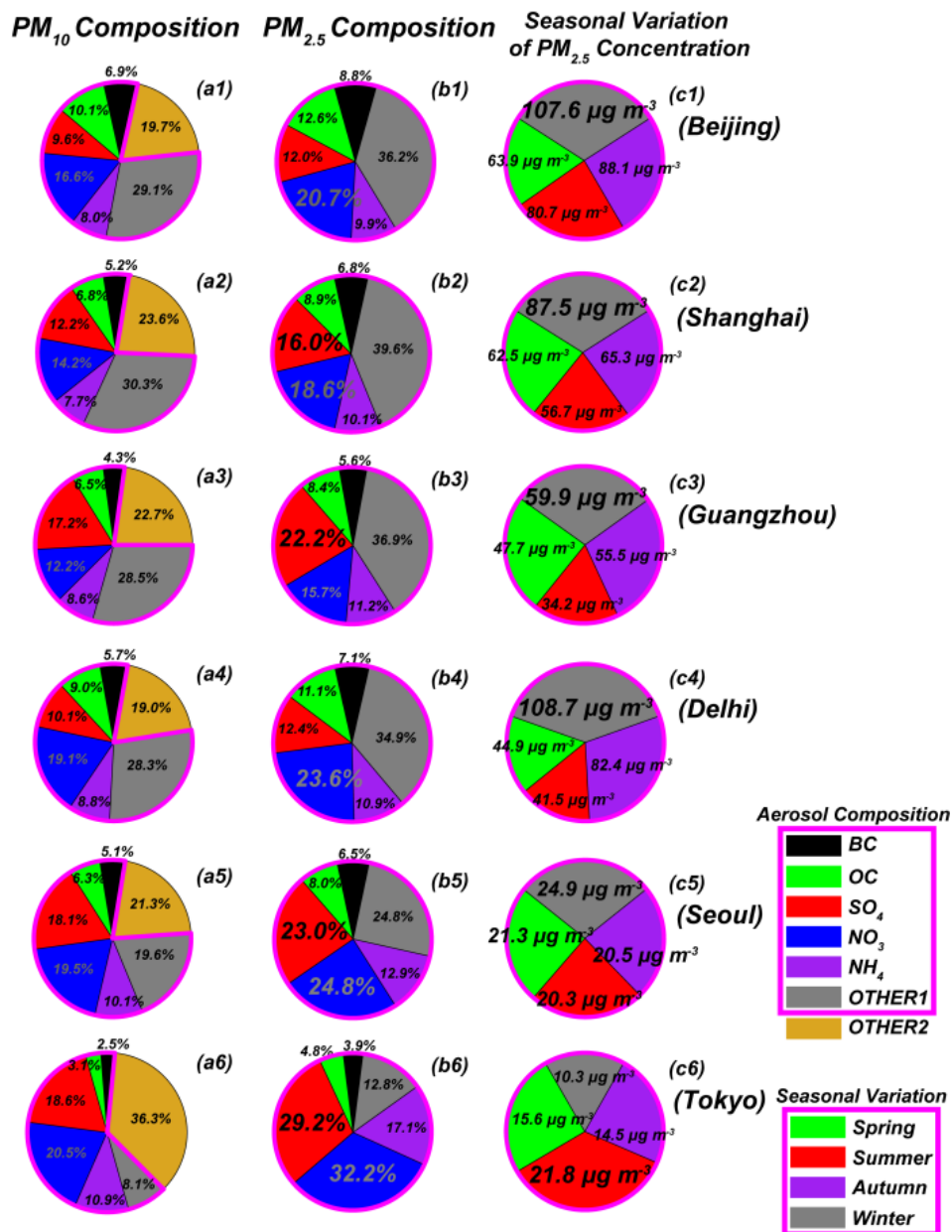


Figure 20: (a) Chemical compositions of simulated particle matter (PM) from all participating models and the ensemble mean. (b) The ratio of each composition to PM_{10} and $PM_{2.5}$ from multi-model ensemble mean. PM_{10} includes $PM_{2.5}$ and OTHER2, while $PM_{2.5}$ is composed of BC, OC, SO_4^{2-} , NO_3^- , NH_4^+ and OTHER1. Notably, OTHER2 cannot be calculated in M13 because PM_{10} concentration has not been submitted. OC is not available in M7, so we leave it into OTHER1. BC and OC are not available in M9 and these concentrations are grouped into OTHER1.



5 Figure 21: Chemical compositions of simulated particle matter in six metropolitans. (a) Beijing, (b) Shanghai, (c) Guangzhou, (d) Delhi, (e) Seoul and (f) Tokyo.



5 **Figure 22: Ratios of chemical compositions to PM₁₀ (a1-a6) and PM_{2.5} (b1-b6) from multi-model ensemble mean in six cities. Seasonal variations of PM_{2.5} concentrations are also shown (c1-c6).**